Estrogen Receptor β Activation Inhibits Colitis by Promoting NLRP6-Mediated Autophagy

Wentao Fan
Nanjing Agricultural University
Chenchen Ding
Nanjing Agricultural University
Shuihui Liu
Nanjing Agricultural University
Xiaona Gao
Nanjing Agricultural University
Xiaofei Shen
Nanjing Drum Tower Hospital
Marthe De Boevre
Ghent University https://orcid.org/0000-0002-6151-5126
Zhangshan Gao
Nanjing Agricultural University
Mengcong Li
Nanjing Agricultural University
Shuo Zhang
Nanjing Agricultural University
Yufan Miao
Nanjing Agricultural University
Wenxian Guan
Nanjing Drum Tower Hospital
Guangliang Liu
Chinese Academy of Agricultural Sciences
Liping Yan
Nanjing Agricultural University
Sarah DeSaeger
Ghent University
Suquan Song (suquan.song@njau.edu.cn)
Nanjing Agricultural University

Article

Keywords: Estrogen receptor β (ERβ), NLRP6, colitis, autophagy

Posted Date: July 26th, 2021

DOI: https://doi.org/10.21203/rs.3.rs-750908/v1

Estrogen Receptor β Activation Inhibits Colitis by Promoting NLRP6-Mediated Autophagy

Wentao Fan[1, 3, †], Chenchen Ding[1, 3, †], Shuhui Liu[1, 3, †], Xiaona Gao[1, 3], Xiaofei Shen[2], Marthe De Boevre[4], Zhangshan Gao[1, 3], Mengcong Li [1, 3], Shuo Zhang[1, 3], Yufan Miao[1, 3], Wenxian Guan[2], Guang Liang Liu [5], Liping Yan[1, 3], Sarah De Saeger[4], Suquan Song[1, 3, *]

Affiliations:

[1]MOE Joint International Research Laboratory of Animal Health and Food Safety, College of Veterinary Medicine, Nanjing Agricultural University, Nanjing 210095, China

[2]Department of Gastrointestinal Surgery, Nanjing Drum Tower Hospital, the Affiliated Hospital of Nanjing University Medical School, Nanjing, 210008, China.

[3]Jiangsu Engineering Laboratory of Animal Immunology, Institute of Immunology and College of Veterinary Medicine, Nanjing Agricultural University, Nanjing 210095, China

[4]Centre of Excellence in Mycotoxicology and Public Health, Faculty of Pharmaceutical Sciences, Ghent University, Ottergemsesteenweg 460, B-9000 Ghent, Belgium.

[5]State Key Laboratory of Veterinary Etiological Biology, Lanzhou Veterinary Research Institute, Chinese Academy of Agricultural Sciences, Lanzhou 730046, China

[†]Wentao Fan, Chenchen Ding, and Shuhui Liu contributed equally to this work.

*Corresponding authors. Email: suquan.song@njau.edu.cn.

Competing Interests statement: The authors declare no conflict of interest.

Abstract

Estrogen receptor β (ERβ) and NLRP6 are highly expressed in intestinal tissues. Loss of ERβ and NLRP6 exacerbate colitis in mouse models. However, the underlying mechanisms are incompletely understood. Here, we report that ERβ attenuates inflammation by inducing NLRP6-mediated autophagy. Specifically, ERβ directly activates the NLRP6 gene expression via binding to estrogen responsive element (ERE) of Nlrp6 gene promoter. ERβ also physically interacts with the NLRP6 nucleotide-binding domain and promotes NLRP6 inflammasome assembly. The ERβ-NLRP6 axis then interacts with multiple autophagy-related proteins including ULK1, BECN1, ATG16L1, LC3B, p62 to affect the autophagosome biogenesis and control autophagic flux. Finally, NLRP6-mediated autophagy suppresses the inflammatory response by promoting the K48-linked polyubiquitination of ASC, Casp-1 p20, IL-1β, TNF-α, and prohibitin-2. Thus, ERβ-NLRP6 direct an anti-inflammatory response by promoting autophagy. Our work uncovers an ERβ-NLRP6-autophagy pathway as an unrecognized regulatory mechanism that maintains intestinal epithelial cell homeostasis and facilitates tissue repair in colitis.

Introduction

Inflammatory bowel disease (IBD), including Crohn's disease (CD) and ulcerative colitis, is characterized by inflammation of the intestinal tract of unknown origin, leading to bowel damage and disabilities [1]. Although its pathogenesis is still incompletely understood, IBD is known to arise from a complex interplay of environmental factors, genetic susceptibilities and bacterial dysbiosis that impair intestinal barrier function and culminate in uncontrolled immune responses against luminal triggers [2-4].

Innate immune cell activation and inflammation are controlled autonomously through hardwired receptor-mediated sensory mechanisms and the production of both pro-inflammatory and immunosuppressive mediators. The hematopoietic immune system acts in concert with intestinal epithelial cells (IECs) to regulate immune cell function and local homeostatic and inflammatory responses [5-8]. IECs can function as immune rheostats via sensory mechanisms that induce an immunomodulatory output.

Innate pattern recognition receptors, such as NOD-like receptors (NLRs), are expressed on diverse cell types and recognize damage- and pathogen-associated molecular patterns to activate effector responses [8]. NLR family members form inflammasomes with the adaptor protein "apoptosis associated speck-like protein containing a CARD" (ASC) and effector enzyme pro-caspase-1 to coordinate immune responses during homeostasis and inflammation. IECs express high levels of "NOD-, LRR- and pyrin domain-containing 6" (NLRP6) [9]. NLRP6-deficient mice are susceptible to colitis and show more pronounced inflammation in the colon than

wildtype mice [10]. NLRP6 inflammasome signaling controls intestinal inflammation through a variety of mechanisms, such as modulating the secretion of the pro-inflammatory cytokine interleukin-18 (IL-18), reducing the colonization of pro-colitogenic gut bacteria and promoting secretion of mucus from goblet cells [11-14]. NLRP6 deficiency abrogates autophagy in goblet cells, providing a link between inflammasome activity, autophagy, mucus secretion, and antimicrobial barrier function [15]. Mechanistic studies to assess the ligands of the NLRP6 and how it regulates autophagy and the inflammasome are of significant interest.

The estrogen receptor ERβ is highly expressed in colon [16] and has been shown to play a therapeutic role in IBD [17]. Moreover, subtype-selective ligands that specifically target ERβ may provide a potential treatment for inflammatory disease [18]. Mechanistically, a complete absence of ERβ expression is associated with disrupted tight-junction formation and abnormal colonic structure [19]. The plant compound arctigenin was recently shown to protect mice from colitis by activating ERβ-MLCK/MLC signaling and upregulating the expression of tight junction proteins [20]. In addition, intestinal epithelial ERβ can impact gut microbiota diversity in colitis-induced colorectal cancer [21]. The diverse functions of ERβ in intestinal health and inflammation are incompletely understood. In microglia and astrocytes, an ADIOL-ERβ-CtBP pathway potently inhibits the transcriptional activation of inflammatory response genes [22], suggesting that ERβ could contribute to recovery from colitis by regulating the transcription of inflammation-related genes in IECs.

In this study, we found that ERβ and NLRP6 levels are both reduced in IBD. We show that ERβ directly activates NLRP6 gene expression and interacts with the NLRP6 inflammasome. We found that NLRP6 sequentially interacts with the ULK1, BENC1, ATG16L1 complex, and LC3 during autophagy, which in turn prevents inflammation and colitis. Taken together, these findings reveal an anti-inflammatory role for the NLRP6 inflammasome via promoting autophagy. In addition, our results suggest that ERβ could be a potential therapeutic target for the treatment of inflammatory diseases related to NLRP6 inflammasome activation.

Results

ERβ inhibits colitis via NLRP6

ERβ and NLRP6 are key mediators of intestinal homeostasis and inflammation, yet their cellular partners and molecular mechanisms remain poorly understood. To investigate how ERβ contributes to IBD, we examined the role of ERβ loss in acute experimental colitis by challenging mice with dextran sodium sulfate (DSS). Compared to WT mice, *Esr2*$^{-/-}$ mice showed increased susceptibility to DSS, as evidenced by reduced body weight (Fig. S1A), and shorter colons due to inflammatory edema (Fig. S1B). In addition, we observed a massive infiltration of inflammatory cells together with mucosal damage in the colon of *Esr2*$^{-/-}$ mice compared to WT mice (Fig. S1C).

Importantly, NLRP6 protein levels were reduced in *Esr2*$^{-/-}$ compared to colon tissue from DSS-treated WT mice, with the increased ASC and Casp-1 p20 (Fig. 1A). ELISA analysis revealed increased levels of IL-1β and TNF-α, but not IL-1α, IL-6, and IL-8,

in *Esr2*$^{-/-}$ mice relative to WT mice treated with DSS (Fig. 1B). Thus, total loss of ERβ results in more severe DSS-induced colitis with reduced NLRP6 expression. We then treated WT mice with DSS followed by intraperitoneal (i.p.) injection of IL-1β or TNF-α, with or without the selective ERβ agonist ERB-041. ERB-041-treated WT mice were highly protected from IL-1β- or TNF-α induced colitis compared to the untreated mice (Fig. 1C). At day 12, IL-1β or TNF-α treated mice exhibited macroscopic indications of severe intestinal inflammation with extensive bleeding throughout the intestine and significant shortening of the colon, whereas the intestines of mice receiving ERB-041 appeared normal (Fig. 1D). Furthermore, the colons of ERB-041-treated mice exhibited increased structural integrity and reduced immune cell infiltration compared to those from untreated mice (Fig. S1D), which correlated with decreased levels of IL-1β and TNF-α (Fig. S1E). We noticed that ERB-041 treated mice showed higher intestinal expression of ERβ and NLRP6 compared to untreated mice, with the decreased ASC and Casp-1 p20 (Fig. S1F). Thus, ERβ signaling leads to reduced inflammation, increased NLRP6 expression and decreased pro-inflammatory cytokine levels (IL-1β and TNF-α) in mouse models of colitis.

These data imply that ERβ-mediated induction of NLRP6 expression prevents IL-1β/TNF-α-mediated inflammation in colonic tissues. To test this hypothesis, first we used DSS to induce acute colitis in WT and *Nlrp6*$^{-/-}$ mice. As expected, *Nlrp6*$^{-/-}$ mice exhibited hyper-susceptibility to DSS-induced colitis: body weights and colon lengths were significantly decreased in the *Nlrp6*$^{-/-}$ mice compared to WT mice (Fig. S1 G and H). Furthermore, compared to WT mice, *Nlrp6*$^{-/-}$ mice exhibited greater submucosal

edema, more extensive damage to the surface mucosa and ulceration, and markedly elevated levels of pro-inflammatory cytokines (IL-1β and TNF-α), indicative of an excessive inflammatory response (Fig. S1 I and J). In line with these results, the expression of ASC and Casp-1 p20 was increased in *Nlrp6*$^{-/-}$ compared to WT mice (Fig. S1K). These data verify that NLRP6 deficiency leads to severe colonic inflammation and increased disruption of the epithelial barrier.

We treated NLRP6-deficient mice with ERB-041 to determine whether ERβ signaling reduces inflammation by up regulating NLRP6. Briefly, we treated mice with DSS for 7 days followed by ERB-041 for 5 days. ERB-041 treatment of DSS-treated WT mice mitigated colitis and restored colonic histology to normal. In contrast, ERB-041 treatment did not affect DSS-treated *Nlrp6*$^{-/-}$ mice, which showed significant weight loss, reduced colon length and a high degree of inflammation, characterized by immune cell infiltration, crypt hyperplasia, and epithelial erosions, regardless of ERB-041 treatment (Fig. 1E-G). In addition, the levels of pro-inflammatory cytokines, including IL-1β and TNF-α, were similar in the colons of DSS-treated *Nlrp6*$^{-/-}$ mice, with or without ERB-041 treatment (Fig. 1H). ERB-041 treatment of DSS-treated WT mice led to increased expression of NLRP6 and reduced expression of the inflammasome ligands ASC and Casp-1 p20 (Fig. 1I), consistent with reduced activation of the inflammation upon ERB-041 treatment of WT mice; this effect was abolished in *Nlrp6*$^{-/-}$ mice. Overall, these data suggest that loss of NLRP6 prevents the ERB-041-mediated attenuation of both colitis and inflammasome activation. Based on

these findings, we propose that ERβ signaling inhibits the inflammasome, and in turn colitis, via NLRP6.

ERβ directly binds and activates the Nlrp6 gene promoter

To investigate the mechanism of ERβ-mediated activation of NLRP6, we first examined how ERβ signaling affects the inflammatory response in normal human colon epithelial cells (NCM-460). Briefly, we exposed NCM-460 cells to DSS and treated them with ERB-041 or vehicle (DMSO). ERB-041 treatment mitigated the effects of DSS, including rescuing cell viability, reducing the levels of IL-1β- and TNF-α (Fig. 2A), restoring the expression of ERβ and NLRP6, and decreasing the expression of the inflammasome ligands ASC and Casp-1 p20 (Fig. 2B). DSS treatment further decreased cell viability and increased the levels of IL-1β- and TNF-α in NLRP6 knockdown (Sh-NLRP6) NCM-460 cells (Fig. S2A-a). DSS treatment of Sh-NLRP6 cells also led to elevated expression of ASC and Casp-1 p20 (Fig. S2A-b). Notably, the anti-inflammatory effects of ERB-041 were less dramatic in Sh-NLRP6 cells (Fig. S2A). We confirmed these observations in ERβ knockdown (Sh-ERβ) cells, which showed decrease of NLRP6 expression (Fig. S2B). These observations further suggest that ERβ regulates NLRP6 expression and inflammasome signaling in DSS-induced IECs inflammation.

We detected an ERE (AGGTCANNNTGACCT) in the *Nlrp6* promoter and hypothesized that ERβ directly regulates *Nlrp6* gene expression. To test this hypothesis, we designed *Nlrp6* probe and performed gel shift assays (Fig. 2C) and ChIP-qPCR (Fig. 2D) in NCM-460 cells. We observed an obvious gel shift of the NLRP6 probe with

nuclear extract isolated from NCM-460 cells stimulated with ERB-041, but not with extracts from those stimulated with the ERα agonist PPT. In addition, we found that ERβ interacted with the *Nlrp6* promoter by ChIP-qPCR. We also designed a reporter assay with the *Nlrp6* promoter driving luciferase expression and found that ERB-041 treatment enhanced luciferase expression in NCM-460 cells, whereas PPT treatment did not (Fig. 2E). Finally, ERβ and NLRP6 expression were found to be dramatically increased after ERB-041 treatment on levels of mRNA, whereas ASC and caspase-1 expression were not (Fig. 2F and Fig. S2C). These data suggest ERβ directly targets and regulates *Nlrp6* gene expression in colon epithelial cells.

ERβ is a component of the NLRP6 inflammasome in IECs

It has been suggested that non-genomic actions of the ERβ can activate intracellular signaling cascades [23]. Interestingly, we found that purified GST-ERβ could pull down Flag-tagged NLRP6 (Fig. 2G). To define which domain of NLRP6 interacts with ERβ, we transfected HEK293T cells with Flag-EGFP-tagged NLRP6 mutants. As shown in Fig. 2H, the interaction of NLRP6 and ERβ was dependent upon the nucleotide-binding domain (NBD) of NLRP6. To uncover a potential role for ERβ signaling in NLRP6 inflammasome assembly, we used NCM-460 cells expressing NLRP6-mCherry and ASC-EGFP. We observed significant colocalization of NLRP6 inflammasome (NLRP6 and ASC) in NCM-460 cells treated with ERB-041 but not in those treated with PPT (Fig. 2I). In addition, DSS treatment reduced the colocalization of NLRP6 and ASC in NCM-460 cells, which was then enhanced by ERB-041 treatment (Fig. S2D). These data suggest that ERβ signaling promotes NLRP6

193 inflammasome assembly. Furthermore, ASC and Pro-casp-1 co-immunoprecipitated
194 with endogenous NLRP6 and ERβ from untreated NCM-460 cells (Fig. S2E).

195 To extend our analysis, we performed immunofluorescence of colon tissue from
196 ERB-041- and PPT-treated WT mice. Colon tissue from ERB-041-treated mice
197 displayed ASC specks, most of which colocalized with NLRP6 puncta, consistent with
198 NLRP6 inflammasome formation in NCM-460 cells (Fig. 2J). In contrast, ASC speck-
199 NLRP6 puncta colocalization was not observed in the colons of untreated and PPT-
200 treated mice. We repeated this analysis with WT and *Esr2*$^{-/-}$ mice treated with DSS. In
201 contrast to DSS-treated WT mice, DSS-treated *Esr2*$^{-/-}$ mice did not exhibit NLRP6
202 inflammasome formation due to loss of NLRP6 expression (Fig. S2F). Overall, our
203 results suggest a direct interaction between ERβ and NLRP6, which represent a new
204 pathway for NLRP6 inflammasome assembly.

205 **The ERβ-NLRP6 axis reduces mitochondrial damage during inflammation**

206 Next, we examined the roles of ERβ and NLRP6 in response to cytokine-induced
207 inflammation of epithelial cells. IL-1β or TNF-α treatment of DSS-treated NCM-460
208 cells led to reduced cell viability and increased inflammation, and both phenotypes were
209 mitigated by co-treatment with ERB-041 (Fig. 3A-a). Knockdown of NLRP6 or ERβ
210 blocked the anti-inflammatory effects of ERB-041 treatment (Fig. 3A-b, c).

211 Mitochondria have critical roles in immunity, and damaged mitochondrial DNA can
212 induce the expression of TNF-α [24]. In addition, mitochondrial ROS (mtROS) can
213 accelerate the maturation of IL-1β [25]. Cytokine secretion can, in turn, induce

mitochondrial damage and mtROS production, suggesting a feedback loop between inflammation and mitochondria [26-28]. Therefore, we examined whether the ERβ-NLRP6 pathway plays a role in mitochondrial damage and ROS production during inflammation. We treated NCM-460 cells with DSS, together with IL-1β or TNF-α, and observed bipolar perinuclear mitochondrial clustering, which was inhibited by treatment with ERB-041. Knockdown of NLRP6 or ERβ counteracted the protective effect of ERB-041 (Fig. S3A). To detect mitochondrial ROS production, we FACS sorted live cells stained with the MitoSOX™ Red superoxide indicator. We observed increased MitoSOX staining in NCM-460 cells stimulated with IL-1β or TNF-α, as expected. Importantly, ERB-041 treatment decreased the production of mtROS, whereas knockdown of NLRP6 or ERβ eliminated the effects of ERB-041 (Fig. 3B). We also examined the morphology of mitochondria in control and DSS-treated cells by transmission electron microscopy, and classified mitochondria as normal (cristae are maintained), or damaged (mildly swollen and increased mitochondria fission or fusion, severely swollen and >70% of cristae are missing, or highly dysmorphic and electron dense). We found that DSS-treated cells contained a high proportion of damaged mitochondria, which was exacerbated by the addition of IL-1β or TNF-α, and this was reversed by ERB-041 treatment (Fig. 3C and Fig. S3B).

Autophagy can inhibit the accumulation of dysfunctional mitochondria and reduce the generation of mtROS to regulate inflammation [29]. To assess autophagy during inflammation, we examined autophagosomes in ultrastructural images of NCM-460 cells. We found that ERB-041 treatment increased the number of autophagosomes in

cells treated with DSS as well as with IL-1β or TNF-α (Fig. 3D and Fig. S3C). In addition, exposure to DSS as well as IL-1β or TNF-α induced atypical cell death associated with formation of cytoplasmic vacuoles. Most of these expanded vacuoles contained indigestible debris and remnants of organelles [30].

To determine if ERB-041 reduces inflammation by increasing autophagy, we assessed the effect of ERB-041 after blocking autophagy. We found that ERB-041 lost the role in improving cell viability and reducing inflammation when the autophagy inhibitor 3-Methyladenine (3-MA) added in NCM-460 cells (Fig. 3E). Active mitochondrial staining with MitoTracker Red revealed that ERB-041 failed to suppress the bipolar perinuclear mitochondrial clustering after 3-MA treatment (Fig. S3D).

Overall, our results suggest that ERβ signaling in intestinal epithelial cells reduces inflammation and decreases mitochondrial damage by affecting autophagy. Moreover, this protective effect of ERβ signaling on mitochondria requires NLRP6.

ERβ signaling controls autophagic flux via NLRP6

Next, we examined the levels of autophagy proteins in NCM-460 cells 48 h after DSS challenge with ERB-041 treatment. As shown in Fig. 4A and Fig. S4A, in line with previous observations, DSS treatment of NCM-460 cells reduced the levels of several autophagy-related proteins (ULK1, BECN1, ATG16L1, LC3). The levels of p62, which delivers autophagic cargo and is degraded in the process [31], were also reduced. However, the levels of prohibitin 2 (PHB2), an inner mitochondrial membrane that targets mitochondria for degradation were increased [32]. ERB-041 treatment restored

257 autophagy protein levels, including p62 expression, in DSS-treated NCM-460 cells,
258 suggesting that ERβ signaling increases autophagy. Knockdown of NLRP6 or ERβ
259 blocked these effects of ERB-041, suggesting that NLRP6 is required for autophagy
260 induction by ERβ signaling. It is worth noting, PHB2 has been identified as a repressor
261 of nuclear estrogen receptor activity [33, 34]. Consistent with these reports, ERB-041
262 significantly decreased PHB2 expression in NCM-460 and Sh-NLRP6 cells but not in
263 Sh-ERβ cells.

264 We also analyzed the expression of autophagy markers in ERβ- or NLRP6-deficient
265 mouse colons (Fig. 4B and Fig. S4B). Compared with WT mice, *Esr2*$^{-/-}$ and *Nlrp6*$^{-/-}$
266 mice had reduced levels of ULK1, BECN1, ATG5, ATG12, ATG16L1, and p62. DSS
267 treatment led to reduced levels of autophagy-related proteins in WT mice, and these
268 proteins remained markedly suppressed in ERβ- or NLRP6-null mice. Furthermore,
269 ERB-041 treatment increased the levels of these proteins in the colons of WT but not
270 *Nlrp6*$^{-/-}$ mice. Together, our data suggest that ERβ signaling reduces inflammation by
271 affecting autophagy via NLRP6.

272 To investigate how NLRP6 and ERβ signaling affect autophagic flux during
273 inflammation, we examined LC3B trafficking using confocal microscopy (Fig. 4C and
274 Fig. S4C). As shown, knockdown of NLRP6 and ERβ appeared to inhibit autophagic
275 flux in control cells, as indicated by an increase in the number of autophagosomes but
276 not of autolysosomes. EGFP-mCherry-LC3B showed low and diffuse cytoplasmic
277 expression in NCM-460 treated with DSS, suggesting that autophagy is inhibited. In
278 contrast, EGFP-mCherry-LC3B showed high and punctate expression treated with

ERB-041, suggesting that autophagy is restored. ERB-041 had no effect on EGFP-mCherry-LC3B localization in DSS-treated Sh-NLRP6 and Sh-ERβ cells. These data suggest that ERβ signaling increases autophagic flux in WT cells and that this effect is abrogated by loss of NLRP6 and ERβ.

NLRP6 and ERβ interact with autophagy-related proteins

Intriguingly, we observed that NLRP6 colocalized with LC3B in NCM-460 cells treated with ERB-041 (Fig. 4D). Moreover, we found that ULK1, ATG5, BECN1, ATG12, ATG16L1, p62, and PHB2 co-immunoprecipitated with both endogenous NLRP6 (Fig. S4D-a) and ERβ (Fig. S4D-b) from untreated NCM-460 cells, and both ERβ and NLRP6 co-immunoprecipitated with LC3 (Fig. S4D-c). To investigate whether ERβ and/or NLRP6 interact directly with autophagy proteins, we performed pull-down assays. We found that purified GST-NLRP6 pulled down many autophagy proteins, except ULK1, from NCM-460 cells (Fig. S4D-a), whereas GST-ERβ did not (Fig. S4D-b). Importantly, the binding of NLRP6 and ERβ to autophagy proteins in NCM-460 cells was partially decreased by DSS but was restored by ERB-041 treatment (Fig. 4E). We infer that NLRP6 interacts directly with autophagy proteins, whereas ERβ interacts indirectly, likely via an NLRP6 complex.

To further investigate the interactions among NLRP6, the autophagy proteins, and damaged mitochondria, we performed immunofluorescence confocal microscopy. Notably, ULK1/BECN1/ATG5/ATG12/ATG16L1 co-localized with NLRP6 on mitochondria in untreated NCM-460 cells (Fig. S4E). Overall, our data suggest that NLRP6 interacts with autophagy proteins and regulates autophagy and/or mitophagy.

To investigate how inflammasome formation affects the interactions between NLRP6, ERβ, and autophagy-related proteins, we analyzed HEK293T cells, which do not express the inflammasome adaptor protein ASC (Fig. 4F-a). We found that ULK1, BECN1, and ATG12 co-immunoprecipitated with NLRP6 (Fig. 4F-b) and ERβ (Fig. S4F-a). In contrast, ATG5, ATG16L1 and PHB2 no longer co-immunoprecipitated with NLRP6 and ERβ. Unexpectedly, p62 co-immunoprecipitated with ERβ, but not with NLRP6. Moreover, ERβ and NLRP6 co-immunoprecipitated with LC3 in HEK293T cells (Fig. S4F-b). To determine whether the autophagy-related proteins-NLRP6 association requires ASC, we performed a Co-IP assay using HEK293T cells with Flag-EGFP-tagged ASC. Upon ASC transfection, ATG5, ATG16L1, p62, and PHB2 associated with NLRP6 (Fig. 4F-c). These results suggest that the assembled NLRP6 inflammasome interacts with a greater diversity of autophagy proteins than the individual components.

ERβ affects inflammation by promoting the association between NLRP6 and autophagosomes throughout their Biogenesis

Autophagosome formation is coordinated by at least three critical protein complexes: the ATG1-Atg13-FIP200-Atg101 complex, the ATG6-Atg14-Vps34-Vps15 (class III PI3-kinase) complex, and the Atg12-Atg5-Atg16L1 complex. Additionally, p62 and LC3 are also involved in autophagosome generation[31] *(31)*. We performed live cell imaging to examine the localization of representative factors from each complex (ULK1, BECN1, ATG16L1, p62, and LC3B), fused to mCherry, and of EGFP-NLRP6, in starved NCM-460 cells undergoing autophagy. We found that red autophagy-related

proteins co-localized with green NLRP6 in a highly dynamic process after inducing autophagy by amino acid starvation (Fig. S5, SI videos). Interestingly, EGFP-NLRP6 co-localized with mCherry-ULK1 after 118s (SI Video 1), but took longer to co-localize with mCherry-ATG16L1 and mCherry-LC3B (401s and 425s, respectively, SI Video 2, SI Video 3) and even longer for mCherry-BECN1 and mCherry-p62 (625s and 620s, SI Video 4, SI Video 5). EGFP-NLRP6 co-localized with mCherry-PHB2 after about 474s (SI Video 6), which was similar to the kinetics of co-localization with ATG16L1 and LC3B. The hierarchical analyses of mammalian ATG proteins showed the ULK1 complex appears to be the most upstream factor, followed by the Atg12-Atg5-Atg16L1 complex, LC3, and the BECN1 complex. We found that NLRP6 co-localized with ULK1 rapidly after the initiation of autophagy and was associated with autophagosomes throughout their biogenesis. Interestingly, DSS could postpone this co-localization (Fig. S5, SI Videos 7-12) to impede autophagy formation, substrate degradation. Importantly, ERB-041 accelerated autophagy formation by reducing the time required for co-localization (Fig. S5, SI Videos 13-18).

The autophagic adaptor p62 links ubiquitinated substrates to the autophagy pathway. Post-translational modification of proteins by covalent conjugation of ubiquitin (Ub) plays a crucial role in regulating inflammation. We found that ASC, Casp-1 p20, IL-1β, TNF-α, and PHB2 immunoprecipitated from untreated NCM-460 cells were all polyubiquitinated (Fig. 5A). The ubiquitin-binding domain of p62 has a preference for polyubiquitin chains[31] *(31)*, and we found that LC3 and p62 co-immunoprecipitated with these proteins (Fig. 5B). These results suggest that the inflammasome, cytokines,

and damaged mitochondria are polyubiquitinated and suggest that these aggregates can be targeted by p62 to suppress inflammation. Consistent with this notion, DSS inhibited the co-immunoprecipitation of ASC, Casp-1 p20, IL-1β, TNF-α, and PHB2 with LC3 and p62 (Fig. 5C), but this inhibition could be reversed by ERB-041. Next, we determined whether ASC, Casp-1 p20, IL-1β, TNF-α, and PHB2 undergo K48-linked polyubiquitination by using K48-specific ubiquitin antibodies. Indeed, these proteins underwent K48-linked polyubiquitination. Moreover, K48-linked ubiquitination of ASC, Casp-1 p20, IL-1β, TNF-α, and PHB2 was diminished in DSS treatment, which was significantly prevented by ERB-041 (Fig. 5D). These data suggest that ERβ-NLRP6-mediated positive regulation of autophagic flux might help to resolve DSS induced inflammation.

NLRP6 is required for Rap-induced recovery from inflammation

To further confirm the role of autophagy in ERβ-NLRP6 mediated anti-inflammatory effects, DSS-treated WT mice were administered ERB-041 for 5 days and treated concomitantly with the autophagy inhibitor 3-MA. Mice receiving ERB-041 had less severe colitis compared to mice receiving saline, as evidenced by a significant reduction in weight loss and colon shortening; however, these effects were attenuated by 3-MA, and mice treated with 3-MA alone had severe colitis (Fig. 6A, B). Colons isolated from mice DSS-treated subsequently treated with ERB-041 showed intact crypts in large areas without extensive infiltration or thickening of the mucosa (Fig. 6C) as well as reduced IL-1β and TNF-α secretion, suggesting suppression of inflammation (Fig. 6D and Fig. S6A). At the protein level, ERB-041-treated mice showed reduced ASC and

Casp-1 p20 expression, as well as increased ATG16L1 and p62 expression, when compared with saline-treated mice (Fig. 6E). 3-MA abrogated the effects of ERB-041 and increased inflammation by all the parameters we measured (Fig. 6B-E).

Inhibition of mTOR is known to stimulate autophagy activity. Treatment with rapamycin (Rap), a pharmacological inhibitor of mTOR, can activate autophagy and reduce active colitis [35, 36] (Fig. S6B). To determine whether the activation of autophagy could still protect *Nlrp6*$^{-/-}$ mice from colitis, we treated *Nlrp6*$^{-/-}$ mice with 3% DSS for 7 days followed by a 5-days treatment with saline or Rap. Saline- and Rap-treated mice appeared to recover similarly based on weight loss, colon length, and inflammatory cytokine levels (Fig. 6F, G and Fig. S6C-a, b). Unexpectedly, 5 Rap-treated mice (n = 7) and 3 saline-treated mice (n = 6) did not survive (Fig. 6H). These Rap-treated mice did not recover from colitis, indicated by the presence of inflammatory infiltrates, crypt erosion, and the loss of tissue architecture (Fig. 6I). Interestingly, we found that Rap-treated *Nlrp6*$^{-/-}$ mice did not exhibited activation of autophagy, which evidenced by unchanged levels of autophagy related proteins (ULK1, BECN1, ATG5, ATG16L1, p62, and PHB2) (Fig. 6J). Accordingly, Casp-1 p20 and ASC expression were not significantly different between saline-treated and Rap-treated *Nlrp6*$^{-/-}$ mice (Fig. S6C-c). These results suggest that NLRP6 is required to induce autophagy in colitis.

Discussion

Our results reveal that ERβ activation can inhibit colitis by promoting NLRP6-mediated autophagy. We found that ERβ can positively regulate NLRP6 transcription and

389 facilitate NLRP6 inflammasome assembly. In response to NLRP6, cells can be
390 rendered hyperactivated, rather than death, by induction of autophagy and removal of
391 damaged mitochondria and ROS. We provide evidence that autolysosome formation
392 and substrate degradation are NLRP6 inflammasome-dependent. We show that NLRP6
393 interacts with ULK1 after the initiation of autophagy, and then in chronological order
394 with the ATG proteins during autophagosome assembly. Our data suggest that ERβ-
395 NLRP6 inflammasome-triggered autophagy is an anti-inflammatory mechanism that
396 promotes cell survival by capturing and degrading inflammasomes, damaged
397 mitochondria, and cytokines via ubiquitination.

398 Chronic inflammatory conditions are associated with the prolonged release of
399 inflammatory mediators and the activation of harmful signal-transduction pathways
400 [37]. We found that DSS-treated *Esr2*$^{-/-}$ mice had lower NLRP6 expression and higher
401 IL-1β and TNF-α production. These results suggest that ERβ signaling might inhibit
402 inflammation and colitis via NLRP6. In contrast, ERβ activity is reported to be
403 enhanced in endometriotic tissues to evade endogenous immune surveillance and
404 promote cell survival [38]. Such conflicting findings may be attributed to ERβ-specific
405 expression in different disease types and disease stages. These findings suggest that
406 selective targeting of ERβ in disease tissues might represent a potential therapeutic
407 strategy for hormone-dependent diseases [39]. Our work also uncovered that ERβ, but
408 not ERα, directly binds to ERE in the NLRP6 promoter to promote transcription.
409 Furthermore, we observed rapid activation and formation of the NLRP6 inflammasome
410 complex due to the interaction between ERβ and NLRP6 NBD. As reported, in the

absence of ligands, NLRs may possess an autoinhibited conformation in which the NBD and LRR are in a closed conformation. On ligand engagement, the NBD and LRR transit into an open conformation to assemble into ring-like oligomers [40]. Thus the binding of ERβ with NLRP6 NBD may lead to conformation changes that overcome the autoinhibition, leading to recruitment of ASC and inflammasome activation. Thus, ERβ directly regulates NLRP6 inflammasome signaling pathways via a variety of mechanisms.

NLRP6 is implicated in activating caspase-1 and promoting IL-18 production in epithelial cells, which directly promotes goblet cell dysfunction during colitis, leading to a breakdown of the mucosal barrier [41, 42]. However, the deubiquitinase Cyld was recently shown to prevent excessive IL-18 production in the colonic mucosa by deubiquitinating NLRP6. The deubiquitination inhibited the NLRP6-ASC inflammasome complex as well as intestinal inflammation [43]. Gene ontogeny analyses have uncovered a link between NLRP6 and IEC repair [44]. These conflicting results have raised much discussion in the field, and the role of NLRP6 in intestinal homeostasis and inflammation remains unresolved. We demonstrate here that NLRP6-deficient mice treated with DSS exhibited significant inflammation and deterioration of tissue integrity within the colon. Moreover, ERβ-specific agonists had no obvious effect on DSS-induced colitis in *Nlrp6*$^{-/-}$ mice. These results suggest that ERβ-NLRP6 axis functions in inflammation and IECs repair. Furthermore, we confirmed that the ERβ-NLRP6 axis inhibited IL-1β and TNF-α production, enhanced IEC viability, reduced mitochondrial damage and decreased mtROS production. More importantly, the ERβ-

NLRP6 axis induced autophagosome formation. ERβ was recently reported to promote autophagy through down regulating mTOR or BNIP3 protein in cancerous colonocytes [45]. Any factor that hinders autophagy, whether it is ATG gene ablation or pharmacological intervention, can lead to increased inflammation [46]. Cells lacking mitophagy will accumulate damaged mitochondria, which can generate mtROS that promote cell damage and death [47, 48]. Thus, it is reasonable to speculate that the ERβ-NLRP6 complex regulates the assembly of the autophagosome machinery to guard cellular homeostasis.

Autophagy proceeds through five main phases – initiation, nucleation, elongation, fusion, and degradation. In canonical autophagic responses, ULK1 encodes a protein kinase that is inhibited by mTOR complex 1 (mTORC1), and inhibition of mTOR leads to activation of ULK1 and initiation of autophagy. Autophagosome nucleation requires a complex that contains BECN1 [49], which produces nascent membranes. During phagophore expansion, ATG7 and ATG10 sequentially catalyze the formation of ATG12-ATG5-ATG16L1 complexes. ATG4, ATG7 and ATG3 jointly cleave the precursors of LC3-like proteins into mature forms, then conjugate them to phosphatidylethanolamine, and recruit autophagosomes with the support of WIPI protein. LC3B enables autophagosomes to bind autophagic substrates and/or proteins that mediate cargo selectivity (including p62). On closure, autophagosomes fuse with lysosomes to generate autolysosomes. Luminal acidification then occurs, which activates the lysosomal hydrolases and primes substrate degradation [50].

We found that DSS treatment resulted in reduced levels of the core autophagy proteins. However, ERβ activation recruited the autophagy proteins and promoted autophagy flux in IECs. Intriguingly, both ERβ and NLRP6 interacted with core ATG proteins in IECs, however, in HEK293T cells, which lack the inflammasome component ASC, they did not interact with ATG16L1, LC3, and p62. These data suggest that ERβ and NLRP6 are required throughout the autophagy process, and that autophagosome membrane expansion and abnormal substrate removal (ubiquitination) are NLRP6 inflammasome-dependent.

In terms of autophagic puncta formation, the ULK1 complex is the most upstream unit, required for the formation of the BECN1 complex. The ATG12-ATG5-ATG16L1 complex and LC3 are downstream of these factors [51]. Although the ATG proteins are functionally interdependent, the chronological order of their recruitment to autophagosome formation sites is incompletely understood [52]. To better understand the complicated mechanism of ATG protein recruitment, it is essential to determine the temporal interaction relationships between NLRP6 and ATG proteins during autophagosome formation. Our findings revealed that the NLRP6 was recruited to the ULK1 complex first and subsequently interacted in order with ATG16L1, LC3, and PHB2. Finally, the BECN1 complex and p62 simultaneously interacted with NLRP6. Although ATG16L1, LC3, and BECN1 have different positions in the genetic hierarchy, the interaction of NLRP6 with ATG16L1, LC3, and PHB2 precedes the interaction with BECN1 and p62. Therefore, we inferred that NLRP6 promotes ATG16L1 complex and LC3 complex formation at an early phase to prepare for the elongation of the

phagophore membrane. Furthermore, NLRP6 moves in concert with the BECN1 complex and p62 in autophagy activation, which suggests a model that the to-be-degraded substrates (damaged mitochondria, inflammasome, cytokines) recruit the machinery necessary for the de novo formation of an autophagosome, rather than being ‘‘recognized’’ by pre-formed isolation membrane.

Methods

Study design

The aim of this study was to characterize a mechanism of inhibition of colitis by the ERβ-NLRP6-autophagy pathway. We studied ERβ-mediated NLRP6 inflammasome activation *in vivo* using colitis models in mice. We further characterized the ERβ-mediated NLRP6 inflammasome activation in human epithelial cells. ERβ, an important transcription factor, was found to be directly regulating NLRP6 gene expression and NLRP6 inflammasome assembling. Finally, we demonstrated that ERβ-NLRP6 inhibited inflammation by promoting autopahgy. Experiments were performed with littermate controls, using males. Animals were randomized, and the majority of analysis was done in a blinded fashion. Sample sizes varied depending on the goal of each experiments (i.e., dissection at one or multiple time points, *in vitro* cultures, etc.) and expected effect sizes, and numbers of animals and statistical analysis methods are thus given in each figure for every experimental setup. No animals were excluded from analyses. Catalog numbers and the description of different primers, antibodies, and kits used throughout the study can be found as an additional technical sheet (Dataset 1).

Animals

Animals were used in accordance with the guidelines for care and use of experimental animals issued by the Nanjing Agricultural University (Permission Number: SYXK (Su) 2017-0007). Dppa3-Cre mice were from Shanghai Model Organisms Center Inc and crossed with *Esr2*$^{flox/flox}$ mice (TOS160106CC1, Cyagen) to generate *Esr2*$^{-/-}$ mice. *Nlrp6*$^{-/-}$ (*Nlrp6*^{tm1cyagen}) mice were generated by deleting exons 1-7 with a neomycin selection cassette. Genotyping was performed on DNA isolated from the tails of 2-week-old mice. Wild-type male mice, ERβ-deficient and NLRP6-deficient male mice of 6-10 weeks old back-crossed on a C57BL/6 background were used in the experiment. Littermates were used as control, whatever possible. We randomly chose mice from the same or different littermates for experimental group and we did not blind to group allocation during experiments and data analysis. All mice are specific pathogen free and were fed a normal diet and allowed to drink tap water ad libitum. The ARRIVE reporting guidelines was used to report methods and results.

Animal models of colitis

Colitis was induced by 3% DSS (MP Biomedicals, 36,000-50,000 MW) dissolved in drinking water, given ad libitum for 7 consecutive days. The effects of selective ERβ agonist (ERB-041, HY-14933, MedChemExpress), rapamycin (HY-10219, MedChemExpress), 3-MA (HY-19312, MedChemExpress), and IL-1β (Z02985-10, Genscript) or TNF-α (Z03333-10, Genscript) were studied on the colitis model mice by intraperitoneal injection for 5 days.

Necropsy, gross pathology examination and histological analysis

On the last day of the study, mice were anesthetized and necropsied. Colons were removed for gross pathologic evaluation. Colon lengths from all groups were recorded. Colons were flushed with ice-cold PBS and immediately fixed in 4% buffered formalin. Fixed tissues were further transferred into an automatic tissue processor (Leica, Germany). Sections of 5 μm were stained with hematoxylin and eosin (H&E). All slides were photographed by a microscope (Olympus BX53, Japan) in a blinded fashion.

Enzyme-linked immunosorbent assays (ELISA)

Mouse IL-1α ELISA kit (Ml002273, Mlbio), Mouse IL-1β ELISA kit (Ml063132, Mlbio), Mouse IL-6 ELISA kit (Ml063159, Mlbio), Mouse IL-8 ELISA kit (Ml063162, Mlbio), Mouse TNF-α ELISA kit (Ml002095, Mlbio), Human IL-1β ELISA kit (Ml028611, Mlbio), Human TNF-α ELISA kit (Ml037301, Mlbio) were used for cytokines measured, respectively, according to the manufacturer's instructions.

Cell lines

Normal human colon mucosal epithelial cell line (NCM-460) was purchased from INCELL and cultured in Dulbecco's modified Eagle's medium (DMEM) (no phenol red, 21063029, Thermo Fisher Scientific) supplemented with 10% (v/v) charcoal-stripped fetal bovine serum (FBS) (12676029, Gibco), 1% (v/v) penicillin-streptomycin (1 mg/mL) at 37°C in a 95% humidified atmosphere with 5% CO_2.

HEK293T cells obtained from ATCC were grown in DMEM, supplemented with 10% FBS and 1% penicillin-streptomycin at 37°C in 5% CO_2 at 100% humidity.

Co-immunoprecipitations and western blotting analysis

Rabbit polyclonal anti-ERβ (OM252100, OmnimAbs) (1:500), Rabbit polyclonal anti-NLRP6 (OM264589, OmnimAbs) (1:500), Anti-Flag (M2 F3165, Sigma-Aldrich) (1:8000), Rabbit polyclonal anti-ASC (OM122624, OmnimAbs; SC-514414, Santa Cruz) (1:500), Mouse monoclonal anti-Casp-1 p20 (SC-398715, Santa Cruz Biotechnology) (1:300), Mouse monoclonal anti-Procaspase-1(SC-392736, Santa Cruz Biotechnology) (1:300), Rabbit monoclonal anti-β-Actin (4970S, Cell Signaling Technology) (1:1000), Rabbit polyclonal anti-IL-1β (D220820, Sangon Biotech) (1:1000), Rabbit polyclonal anti-TNFα (D164310, Sangon Biotech) (1:1000), Mouse monoclonal anti-Prohibitin 2 (SC-133094, Santa Cruz Biotechnology) (1:300), Rabbit polyclonal anti-UBB (D220023, Sangon Biotech) (1:250), anti-K48 linkage-specific polyubiquitin (4289S ,Cell Signaling Technology) (1:2000), Rabbit monoclonal anti-ULK1 (8054T, Cell Signaling Technology) (1:1000), Rabbit monoclonal anti-ATG5 (12994T, Cell Signaling Technology) (1:1000), Rabbit monoclonal anti-BECN1 (3495T, Cell Signaling Technology) (1:1000), Rabbit monoclonal anti-ATG12 (4180T, Cell Signaling Technology) (1:1000), Rabbit monoclonal anti-ATG16L1 (8089T, Cell Signaling Technology) (1:1000), Rabbit monoclonal anti-SQSTM1/p62 (8025T, Cell Signaling Technology) (1:1000), Rabbit polyclonal anti-LC3 (14600-1-AP, Proteintech) (1:1000), Mouse monoclonal anti-GST (SC-80998, Santa Cruz Biotechnology) (1:500), Mouse monoclonal anti-IgG (SC-52336, Santa Cruz Biotechnology) (1:500), HRP-Goat Anti-Mouse IgG(H+L) (ab205719, Abcam) (1:5000), HRP-Goat Anti-Rabbit

IgG(H+L) (ab205718, Abcam) (1:8000) were used for immunoblotting their respective proteins.

For co-immunoprecipitation, NCM-460 or HEK293T cells were collected in Buffer A (50mM Tris, 150mM NaCl, 0.5% Triton X-100, PH 7.5) with a protease inhibitor cocktail (HY-K0010, MedChemExpress). Cell lysates were incubated on ice for 30 min and centrifuged at 14,000 × g for 10 min and the supernatants were further diluted with 2 × volume of Buffer A to quantify protein concentration. The diluted lysates were pre-cleared with protein A/G magnetic beads and then incubated with antibodies and protein A/G magnetic beads overnight at 4°C. The precipitated proteins were washed 3 times with buffer A and analyzed by SDS-PAGE and immunoblotting.

To examine ubiquitination of ASC, Casp-1 p20, IL-1β, TNF-α, and PHB2, NCM-460 cells were lysed in lysis buffer. The ubiquitinated proteins were immunoprecipitated with an anti-UBB rabbit polyclonal antibody. Proteins were then blotted onto a 0.45 μm PVDF membrane. Primary antibodies were incubated with the PVDF membrane. Then HRP-Goat Anti-Mouse IgG(H+L) (ab205719, Abcam) and HRP-Goat Anti-Rabbit IgG (H+L) (ab205718, Abcam) were used. Amersham Imager 600 (GE Healthcare，USA) and Alliance Q9 (UVItec, UK) were used to visualize chemo-luminescence. The bands were analyzed by Image J 1.51j8 (National Institutes of Health, USA).

Cell activity

The cells were seeded in 96-well culture plates at appropriate density were first primed with LPS (100 ng/ml) (00497693, Thermo Fisher Scientific) for 4 h, followed by treatment of 3% DSS for 24 h prior to treatment for 48 h with ERB-041 (1 μM) and TNF-α (5 ng/mL) (Z01001-10, Genscript) or IL-1β (10 ng/mL) (Z02922-10, Genscript). The cell activity was tested according to CCK-8 (40203ES76, YEASEN) protocol. The absorbance at 450 nm was obtained by a microplate reader with Gen5 CHS 2.07 software (BioTek, USA).

Generation of knockdown stable cells

pLVX-shRNA2 (PT4052-5, Clontech), psPAX2 (PVT2320, Life Science Market) and pMD2.G (PVT2321, Life Science Market) vectors were purchased from Nova Lifetech Limited (Hongkong, China). Lentivirus-mediated shRNA targeting NLRP6 (5'-GCTGAGCGAGCAGTCACTACA-3'; 5'-GCAGTCACTACAGGAGCTTCA-3') and ERβ (5'-GGAAATGCGTAGAAGGAATTC-3') mRNA sequences were obtained from Genscript Biotech Corporation.

pLVX-shNLRP6/pLVX-shERβ, psPAX2, and pMD2.G were transfected into the HEK239T cells. The supernatant containing lentivirus was harvested after 40 h and then added into the NCM-460 cells. After 24 h, the medium was replaced with fresh medium. 48 h later, cells were cultured in selection medium containing 10 μg/mL puromycin. All these stable transfected cells were tested regularly by western blotting analysis to ensure the efficiency of down-regulation.

Electrophoretic mobility shift assay (EMSA)

Cloned NLRP6 DNA probe (TGTGAGGATGACCAGAGGTCACTCTCATTGCCATCTTGGTTCTGGTGGTTTTGGGCCAGCTTCTTTACACCATTATCAGCAAGGCCTTTATGACCTGTATCTTGTGTCAACCTCCTGTCTCATCCTGTGA) of 130bp containing estrogen receptor binding sites were labeled with biotin using an EMSA probe biotin labeling kit (GS008, Beyotime). After stimulation with ERB-041(HY-14933, MedChemExpress) and PPT (HY-100689, MedChemExpress), the nuclear extract of NCM-460 cells was prepared for DNA-protein binding assays.

Chromatin immunoprecipitation quantitative polymerase chain reaction analysis (ChIP-qPCR)

NCM-460 cells were centrifuged, and then protein-DNA was cross-linked with 1% formaldehyde. The sediment was sonicated on ice, and the chromatin was diluted in lysis buffer without SDS. The chromatin was separated on an agarose gel to check the quality of DNA. IP grade antibodies for ER were used to perform immunoprecipitation. For the negative control, chromatin was incubated with protein G-coated magnetic beads and polyclonal mouse IgG alone. After reverse cross-linking, the released DNA fragments were purified with a QIAquick DNA purification kit (28104, QIAGEN). PCR was performed to identify the existence of the *Nlrp6* gene. Finally, qPCR was performed to quantify the fold enrichment. The results were computed as percent antibody bound per input DNA and then normalized to IgG controls.

Dual luciferase assay

The human *Nlrp6* promoter was cloned into pGL3-Basic (E1751, Promega). NCM-460 cells were seeded in 96-well plates at a concentration of 50,000 cells/well. Then, the constructed pGL3-*Nlrp6* promoter vector together with pRL-TK (E2241, Promega) was transfected into the cells using Lipofectamine 2000 reagent (11668019, Thermo Fisher Scientific). Cell medium was changed after 6 h, and then the special estrogen receptor agonist was added. Firefly luciferase activity was normalized to Renilla luciferase activity.

Real-time PCR analysis

Cells were seeded in a 6-well plate at an appropriate density. After treating with ERB-041 (1 μM) and PPT (1 μM) for 48h, total RNA was isolated using a Total RNA Kit II (OMEGA, R6934), followed by cDNA synthesis using Hifair® II 1st Strand cDNA Synthesis Kit (YEASEN, 11119ES60). Hieff UNICON® qPCR SYBR Green Master Mix (YEASEN, 11198ES03) was used in a 20 μL reaction volume. quantitative real-time PCR was performed on LightCycler96 (Roche). The expression of individual genes was normalized to the expression of β-actin. The primer sequences for the genes were as follows: human *Nlrp6* forward primer, 5′-AAGGAACTGGAGCAACTG-3′; human *Nlrp6* reverse primer, 5′-CGATGAACTGGTAGGTGAC-3′; human *Esr2* forward primer, 5′-TCCATCGCCAGTTATCACATCT-3'; human *Esr2* reverse primer, 5'-CTGGACCAGTAACAGGGCTG-3'; human *ASC* forward primer, 5'-CGTTGAGTGGCTGCTGGATG-3'; human *ASC* reverse primer, 5'-CAGGCTGGTGTGAAACTGAAGAG-3'; human *Caspase-1* forward primer, 5'-ACACCGCCCAGAGCACAAG-3'; human *Caspase*-1 reverse primer, 5'-

TTTCTTCCCACAAATGCCTTCCC-3'; human *β-actin* forward primer, 5'-GGCATCCACGAAACTACCT-3'; human *β-actin* reverse primer, 5'-ATCTTCATTGTGCTGGGTG-3′.

GST pull-down assays

Esr2 (KR709495.1) gene were cloned into pGEX-4T-1(PVT0029, Life Science Market) and expressed as glutathione-s-transferase (GST) fusion proteins in E. coli BL21(DE3) induced by IPTG. The GST-fusion proteins were obtained by ultra-sonication of E. coli BL21(DE3), then GST-fusion proteins were purified by Glutathione MagBeads (L00327, Genscript). *Nlrp6* (NM_001276700.2) amplified from NCM-460 cells' cDNA and cloned at the XhoI and EcoRI sites of the pCAGGS vector to generate the Flag-tagged NLRP6. The primers are 5′-GTGCCCAACAGCATCTCGT-3′ (F) and 5′-CCACAGGGACTTTGACTAGGGT-3′ (R).

HEK293T cells were transfected with Flag-tagged NLRP6 plasmid by Lipofectamine 2000 reagent and were lysed in Buffer A with a protease inhibitor cocktail. The diluted lysates incubated with GST-fusion protein loaded beads for 12 h at 4 °C. Beads were washed 5 times with washing buffer and boiled for 5 min. Centrifuged with 14,000×g for 5min, the supernatant was used for western blotting analysis.

Plasmids and transfection

Human NLRP6 PYD (1-106aa), PYD+NBD (1-564aa), and LRR (727-868aa) genes were amplified from Flag-tagged NLRP6 plasmid. We added EGFP tag to observe the

665 expression of these mutants. HEK293T cells were plated into a 6-well plate overnight.
666 To examine an interaction between ERβ and NLRP6 mutants, cells were transfected for
667 48 h with 5 μg of plasmids expressing PYD, PYD+NBD, and LRR using Lipofectamine
668 2000. The primer sequences for the genes were as follows: PYD forward primer, 5′-
669 GTGCCCAACAGCATCTCGT-3′; PYD reverse primer, 5′-
670 CTTCTTGTACTCGGACACGGA-3′; PYD+NBD forward primer, 5′-
671 ATGGACCAGCCAGAGGCC-3′; PYD+NBD reverse primer, 5′-
672 GCCGAAGTGGCGCTCGATG-3′; LRR forward primer, 5′-
673 ATGACTGACCCACTGTGCCATCTGA-3′; LRR reverse primer, 5′-
674 GTGTGTGATGACCAGATCCGGCTTT-3′;

675 **Colocalization of NLRP6 inflammasome**

676 Cells were co-transfected with EGFP-ASC (2 μg) and mCherry-NLRP6 (2 μg) plasmid
677 according to the manufacturer's protocol, followed by treatment with PPT (1 μM) for
678 48h, ERB-041 (1 μM) for 48 h, 3%DSS for 48h, 3%DSS+ERB-041 (1 μM) for 48 h.
679 The cells were fixed with 4% paraformaldehyde at 37 °C for 30 min and then
680 counterstained with DAPI. The colocalization of NLRP6 and ASC was visualized by
681 confocal immunofluorescence microscopy.

682 **Immunofluorescence**

683 Paraffin-embedded sections of colonic tissues were deparaffinized, rehydrated and
684 incubated with 3% H_2O_2 for 20 minutes to block endogenous peroxidase, then antigens
685 unmasked using 10mM citrate buffer (pH = 6) for 5 minutes. After blocking, slides for

immunofluorescence were incubated with fluorescein-conjugated primary antibodies overnight at 4 °C in the dark and mounted with DAPI Fluoromount-GTM (P36931, Thermo Fisher Scientific) (1:500). Immunofluorescence images were acquired by Zeiss LSM 980 microscope (Zeiss, Germany) with ZEN Connect software. The data were analyzed by ZEN 3.0 (blue edition) software.

The following antibodies were used for immunofluorescence: Mouse monoclonal anti-ASC antibody PE-labeled (SC-514414, Santa Cruz) (1:400) and Mouse monoclonal anti-Procaspase-1 antibody FITC-labeled (SC-392736, Santa Cruz) (1:400). The NLRP6 used in immunofluorescence was labeled by Cy5 dye (A04002, MedChemExpress).

Active mitochondrial assessment

The cells were seeded in 22 mm confocal dishes at an appropriate density. After LPS priming and 3% DSS, ERB-041 (1 μM) and TNF-α (5 ng/mL) (Z01001-10, Genscript) or IL-1β (10 ng/mL) (Z02922-10, Genscript) stimulation, the cells were incubated for 30 min at 37 °C with 250 nM MitoTracker® Red CMXRos Mitochondrial Probe (M7512, Thermo Fisher Scientific). The fluorescence signals were measured by Zeiss microscope (excitation at 579 nm; emission at 599 nm).

Measurement of mitochondrial ROS

The cells were seeded in a 6-well plate at an appropriate density. After LPS priming and 3%DSS, ERB-041 (1μM) and TNF-α (5 ng/mL) (Z01001-10, Genscript) or IL-1β (10 ng/mL) (Z02922-10, Genscript) stimulation, the cells were loaded with 4 μM of

MitoSOX (M36008, Thermo Fisher Scientific) for 20 min. Fluorescence intensity was determined using Flow Cytometer (Beckman, USA) with Accuri C6 software. FlowJo 10.0 FACS software was used for the data analysis.

Transmission electron microscopy

After LPS priming and 3%DSS, ERB-041 (1 μM) and TNF-α (5 ng/mL) (Z01001-10, Genscript) or IL-1β (10 ng/mL) (Z02922-10, Genscript) stimulation, NCM-460 cells were fixed in 2.5% glutaraldehyde (electron microscopy grade) for 5 minutes at room temperature followed by 2 h at 4 °C. The cell samples were prepared for transmission electron microscopy as described previously [53]. The sections were examined using a HITACHI H-7650 at a voltage of 80 kV. To avoid bias, the entire population of mitochondria in each image (number of images = 3) was examined to count the number of abnormal mitochondria. The percentage of abnormal mitochondria was determined by dividing the number of abnormal mitochondria by the total number of mitochondria per image.

pmCherry- EGFP- LC3B assay

Cells were transfected with pmCherry-EGFP-LC3B (PVT10398, Life Science Market) according to the protocol, followed by treatment with DSS for 2 4h, ERB-041 for 48 h. The cells were fixed with 4% paraformaldehyde at 37 °C for 30 min and then counterstained with DAPI. The fluorescence signals were visualized by confocal immunofluorescence microscopy.

Live cell imaging of autophagy events

Stably expressing EGFP-NLRP6 NCM-460 cells were seeded in 22 mm confocal dishes to a confluency of 30-40%. When confluency of cells reached to 60-70%, the transfection complex mix, containing transfection reagent and mCherry-ULK1/BECN1/ATG16L1/p62/LC3B/PHB2 plasmid DNA, was added. After 24h, the medium was aspirated, and the cells were washed with 2 ml of starvation medium 3 times. Confocal dishes were put in the incubation chamber of Zeiss confocal microscope. The video capture was performed after 30 min starvation using a high magnification lens (60×oil). The intensity of excitation light was adjusted to 10-20% of maximum intensity to prevent photo-bleaching. The image acquisition rate was set to 1 frame every 15 sec.

Statistical Analysis

Statistical tests were performed using using GraphPad Prism 7 (GraphPad Software). Results were presented as mean ± SEM. Student's *t*-test was used to compare the difference between two groups for normally distributed data. Two-tailed probabilities were calculated. A one-way ANOVA with Dunnett's test was used to compare the difference between three groups. A two-way ANOVA with Tukey's or Sidak's multiple-comparisons test was used to evaluate experiments involving multiple groups. Probability (P) values of <0.05 were considered significant: $*P < 0.05$, $**P < 0.01$, $***P < 0.001$ and $****P < 0.0001$; n.s., not significant. Survival was analyzed using the Mantel-Cox log-rank test. We estimate the variation within each experimental group and ensure that the variance is similar for groups that are being statistically compared.

Data Availability Statement

All data generated or analyzed during this study are included in this published article (Table S1, Table S2, and Supplemental Material). Source data are provided with this paper (Unprocessed immunoblots).

References

1. Martin JC, Chang C, Boschetti G, Ungaro R, Giri M, Grout JA, *et al.* Single-Cell Analysis of Crohn's Disease Lesions Identifies a Pathogenic Cellular Module Associated with Resistance to Anti-TNF Therapy. *Cell.*; **178**, 1493-1508 (2019).

2. Ananthakrishnan AN, Bernstein CN, Iliopoulos D, Macpherson A, Neurath MF, Ali RAR, *et al.* Environmental triggers in IBD: a review of progress and evidence. *Nat Rev Gastroenterol Hepatol*. **15**, 39-49 (2018).

3. Park JH, Peyrin-Biroulet L, Eisenhut M, Shin JI. IBD immunopathogenesis: A comprehensive review of inflammatory molecules. *Autoimmun Rev*. **16**, 416-426 (2017).

4. Caruso R, Mathes T, Martens EC, Kamada N, Nusrat A, Inohara N, *et al.* A specific gene-microbe interaction drives the development of Crohn's disease-like colitis in mice. *Sci Immunol*. **4**: eaaw4341 (2019).

5. Hoytema van Konijnenburg DP, Reis BS, Pedicord VA, Farache J, Victora GD, Mucida D. Intestinal Epithelial and Intraepithelial T Cell Crosstalk Mediates a Dynamic Response to Infection. *Cell*. **171**, 783-794 (2017).

6. Eftychi C, Schwarzer R, Vlantis K, Wachsmuth L, Basic M, Wagle P, *et al.* Temporally Distinct Functions of the Cytokines IL-12 and IL-23 Drive Chronic Colon Inflammation in Response to Intestinal Barrier Impairment. *Immunity*. **51**: 367-380 (2019).

7. Grizotte-Lake M, Zhong G, Duncan K, Kirkwood J, Iyer N, Smolenski I*, et al.* Commensals Suppress Intestinal Epithelial Cell Retinoic Acid Synthesis to Regulate Interleukin-22 Activity and Prevent Microbial Dysbiosis. *Immunity*. **49**, 1103-1115 (2018).

8. Nowarski R, Jackson R, Flavell RA. The Stromal Intervention: Regulation of Immunity and Inflammation at the Epithelial-Mesenchymal Barrier. *Cell*. **168**, 362-375 (2017).

9. Levy M, Shapiro H, Thaiss CA, Elinav E. NLRP6: A Multifaceted Innate Immune Sensor. *Trends Immunol*. **38**, 248-260 (2017).

10. Chen GY, Liu M, Wang F, Bertin J, Nunez G. A functional role for Nlrp6 in intestinal inflammation and tumorigenesis. *J Immunol*. **186**, 7187-7194 (2011).

11. Lemire P, Robertson SJ, Maughan H, Tattoli I, Streutker CJ, Platnich JM*, et al.* The NLR Protein NLRP6 Does Not Impact Gut Microbiota Composition. *Cell Rep*. **21**, 3653-3661 (2017).

12. Mamantopoulos M, Ronchi F, Van Hauwermeiren F, Vieira-Silva S, Yilmaz B, Martens L*, et al.* Nlrp6-and ASC-Dependent Inflammasomes Do Not Shape the Commensal Gut Microbiota Composition. *Immunity*. **47**, 339 (2017).

13. Hara H, Seregin SS, Yang D, Fukase K, Chamaillard M, Alnemri ES*, et al.* The NLRP6 Inflammasome Recognizes Lipoteichoic Acid and Regulates Gram-Positive Pathogen Infection. *Cell*. **175**, 1651-1664 e1614 (2018).

14. Man SM. Inflammasomes in the gastrointestinal tract: infection, cancer and gut microbiota homeostasis. *Nat Rev Gastroenterol Hepatol*. **15**, 721-737 (2018).

15. Wlodarska M, Thaiss CA, Nowarski R, Henao-Mejia J, Zhang JP, Brown EM*, et al.* NLRP6 inflammasome orchestrates the colonic host-microbial interface by regulating goblet cell mucus secretion. *Cell*. **156**, 1045-1059 (2014).

16. Jacenik D, Cygankiewicz AI, Fichna J, Mokrowiecka A, Malecka-Panas E, Krajewska WM. Estrogen signaling deregulation related with local immune response modulation in irritable bowel syndrome. *Mol Cell Endocrinol*. **471**, 89-96 (2018).

17. Jiang Q, Li WX, Sun JR, Zhu TT, Fan J, Yu LH*, et al.* Inhibitory effect of estrogen receptor beta on P2X3 receptors during inflammation in rats. *Purinergic Signal*. **13**, 105-117 (2017).

18. Warner M, Huang B, Gustafsson JA. Estrogen Receptor β as a Pharmaceutical Target. Trends in *Pharmacological ences*. **38**, 92-99 (2017).

19. Looijer-van Langen M, Hotte N, Dieleman LA, Albert E, Mulder C, Madsen KL. Estrogen receptor-beta signaling modulates epithelial barrier function. *Am J Physiol Gastrointest Liver Physiol*. **300**, G621-G266 (2011).

20. Tao Y, Yue M, Lv C, Yun X, Qiao S, Fang Y*, et al.* Pharmacological activation of ERbeta by arctigenin maintains the integrity of intestinal epithelial barrier in inflammatory bowel diseases. *FASEB J*. **34**, 3069-3090 (2020).

21. Ibrahim A, Hugerth LW, Hases L, Saxena A, Seifert M, Thomas Q*, et al.* Colitis-induced colorectal cancer and intestinal epithelial estrogen receptor beta impact gut microbiota diversity. *Int J Cancer*. **144**, 3086-3098 (2019).

22. Saijo K, Collier JG, Li AC, Katzenellenbogen JA, Glass CK. An ADIOL-ERbeta-CtBP transrepression pathway negatively regulates microglia-mediated inflammation. *Cell*. **145**, 584-595 (2011).

23. Fuentes N, Silveyra P. Estrogen receptor signaling mechanisms. *Adv Protein Chem Struct Biol*. **116**, 135-170 (2019).

24. Zhang JZ, Liu Z, Liu J, Ren JX, Sun TS. Mitochondrial DNA induces inflammation and increases

816 TLR9/NF-kappaB expression in lung tissue. *Int J Mol Med*. **33**, 817-824 (2014).

817 25. Zhou R, Yazdi AS, Menu P, Tschopp J. A role for mitochondria in NLRP3 inflammasome activation.

818 *Nature*. **469**, 221-225 (2011).

819 26. Roca FJ, Whitworth LJ, Redmond S, Jones AA, Ramakrishnan L. TNF Induces Pathogenic

820 Programmed Macrophage Necrosis in Tuberculosis through a Mitochondrial-Lysosomal-

821 Endoplasmic Reticulum Circuit. *Cell*. **178**, 1344-1361 (2019).

822 27. Yu JJ, Nagasu H, Murakami T, Hoang H, Broderick L, Hoffman HM*, et al.* Inflammasome activation

823 leads to Caspase-1-dependent mitochondrial damage and block of mitophagy. *P Natl Acad Sci USA*.

824 **111**, 15514-15519 (2014).

825 28. Mills EL, Kelly B, O'Neill LAJ. Mitochondria are the powerhouses of immunity. *Nat Immunol*. **18**,

826 488-498 (2017).

827 29. Deretic V, Levine B. Autophagy balances inflammation in innate immunity. *Autophagy*. **14**, 243-251

828 (2018).

829 30. Hino H, Iriyama N, Kokuba H, Kazama H, Moriya S, Takano N*, et al.* Abemaciclib induces atypical

830 cell death in cancer cells characterized by formation of cytoplasmic vacuoles derived from lysosomes.

831 *Cancer Sci*. 2020; 111: 2132-2145.

832 31. Galluzzi L, Green DR. Autophagy-Independent Functions of the Autophagy Machinery. *Cell* 2019,

833 **177**(7)**:** 1682-1699.

834 32. Wei YJ, Chiang WC, Sumpter R, Mishra P, Levine B. Prohibitin 2 Is an Inner Mitochondrial

835 Membrane Mitophagy Receptor. *Cell*. **168**, 224-238 (2017).

836 33. Montano MM, Ekena K, Delage-Mourroux R, Chang WR, Martini P, Katzenellenbogen BS. An

837 estrogen receptor-selective coregulator that potentiates the effectiveness of antiestrogens and

838 represses the activity of estrogens. *P Natl Acad Sci USA*. **96**, 6947-6952 (1999).

839 34. McKenna NJ, O'Malley BW. Combinatorial control of gene expression by nuclear receptors and
840 coregulators. *Cell*. **108**, 465-474 (2002).

841 35. Mathur R, Alam MM, Zhao XF, Liao Y, Shen J, Morgan S*, et al.* Induction of autophagy in Cx3cr1
842 + mononuclear cells limits IL-23/IL-22 axis-mediated intestinal fibrosis. *Mucosal Immunology*. **12**,
843 612-623 (2019).

844 36. Liu M, Sun T, Li N, Peng J, Gao WQ. BRG1 attenuates colonic inflammation and tumorigenesis
845 through autophagy-dependent oxidative stress sequestration. *Nat Commun*. **10**, 4614 (2019).

846 37. Liu CH, Abrams ND, Carrick DM, Chander P, Dwyer J, Hamlet MRJ*, et al.* Biomarkers of chronic
847 inflammation in disease development and prevention: challenges and opportunities. *Nat Immunol*.
848 **18**, 1175-1180 (2017).

849 38. Han SJ, Jung SY, Wu SP, Hawkins SM, Park MJ, Kyo S*, et al.* Estrogen Receptor beta Modulates
850 Apoptosis Complexes and the Inflammasome to Drive the Pathogenesis of Endometriosis. *Cell*. **163**,
851 960-974 (2015).

852 39. Thomas C, Gustafsson JA. The different roles of ER subtypes in cancer biology and therapy. *Nat*
853 *Rev Cancer*. **11**, 597-608 (2011).

854 40. Shen C, Lu A, Xie WJ, Ruan J, Negro R, Egelman EH*, et al.* Molecular mechanism for NLRP6
855 inflammasome assembly and activation. *Proc Natl Acad Sci U S A*. **116**, 2052-2057 (2019).

856 41. Elinav E, Strowig T, Kau AL, Henao-Mejia J, Thaiss CA, Booth CJ*, et al.* NLRP6 inflammasome
857 regulates colonic microbial ecology and risk for colitis. *Cell*. **145**, 745-757 (2011).

858 42. Nowarski R, Jackson R, Gagliani N, de Zoete MR, Palm NW, Bailis W*, et al.* Epithelial IL-18
859 Equilibrium Controls Barrier Function in Colitis. *Cell*. **163**, 1444-1456 (2015).

860 43. Mukherjee S, Kumar R, Tsakem Lenou E, Basrur V, Kontoyiannis DL, Ioakeimidis F*, et al.*
861 Deubiquitination of NLRP6 inflammasome by Cyld critically regulates intestinal inflammation. *Nat*
862 *Immunol*. **21**, 626-635 (2020).
863 44. Normand S, Delanoye-Crespin A, Bressenot A, Huot L, Grandjean T, Peyrin-Biroulet L*, et al.* Nod-
864 like receptor pyrin domain-containing protein 6 (NLRP6) controls epithelial self-renewal and
865 colorectal carcinogenesis upon injury. *P Natl Acad Sci USA*. **108**, 9601-9606 (2011).
866 45. Wei Y, Huang C, Wu H, Huang J. Estrogen Receptor Beta (ERβ) Mediated-CyclinD1 Degradation
867 via Autophagy Plays an Anti-Proliferation Role in Colon Cells. *Int J Biol Sci*. **15**, 942-952 (2019).
868 46. Berglund R, Guerreiro-Cacais AO, Adzemovic MZ, Zeitelhofer M, Jagodic M. Microglial
869 autophagy–associated phagocytosis is essential for recovery from neuroinflammation. *Sci Immunol*.
870 **5**, eabb5077 (2020).
871 47. Green D, Levine B. To Be or Not to Be? How Selective Autophagy and Cell Death Govern Cell Fate.
872 *Cell*. **157**, 65-75 (2014).
873 48. Levine B, Kroemer G. Biological Functions of Autophagy Genes: A Disease Perspective. *Cell*. **176**,
874 11-42 (2019).
875 49. Qian X, Li X, Cai Q, Zhang C, Yu Q, Jiang Y*, et al.* Phosphoglycerate Kinase 1 Phosphorylates
876 Beclin1 to Induce Autophagy. *Mol Cell*. **65**, 917-931 (2017).
877 50. Clarke AJ, Simon AK. Autophagy in the renewal, differentiation and homeostasis of immune cells.
878 *Nat Rev Immunol*. **19**, 170-183 (2019).
879 51. Abada A, Elazar Z. Getting ready for building: signaling and autophagosome biogenesis. *EMBO Rep*.
880 **15**, 839-852 (2014).
881 52. Koyama-Honda I, Itakura E, Fujiwara TK, Mizushima N. Temporal analysis of recruitment of

mammalian ATG proteins to the autophagosome formation site. *Autophagy*. **9**, 1491-1499 (2013).

53. Zhong Z, Umemura A, Sanchez-Lopez E, Liang S, Shalapour S, Wong J, *et al.* NF-kappaB Restricts Inflammasome Activation via Elimination of Damaged Mitochondria. *Cell*. **164**, 896-910 (2016).

Acknowledgments

We would like to thank Santa Cruz Technologies and Sangon Biotech for gifts of antibodies; OLYMPUS Life Science for the help of immunofluorescence images; Dr. Angela Andersen (Life Science Editors) for assistance with manuscript preparation.

Conflict of interests

The authors declare no conflict of interest.

Author contributions

S.Q.S. and W.T.F. conceived the project. W.T.F., C C.D., and S.H.L. performed and analyzed most of the experiments. X.F.S., W.X.G., X.N.G., Z.S.G., M.C.L., S.Z., Y.F.M., M.D.B., G.L.L., and S.D.S. provided technical assistance in various experiments. S.Q.S. and W.T.F. interpreted and wrote the manuscript. S.Q.S. and L.P.Y. supervised the project. All authors contributed to the final text and approved it.

Funding

This work was supported by National Key R&D Program (2016YFD0501009 and 2016YFD0501200), the NAU International Cooperation and Cultivation Project (2018-AF-20), the Priority Academic Program Development of Jiangsu Higher Education Institutions, Natural Science Foundation of China (32002345), China Postdoctoral Science Foundation (2020M681650), the State Key Laboratory of Veterinary Etiological Biology (SKLVEB2019KFKT013).

Figures

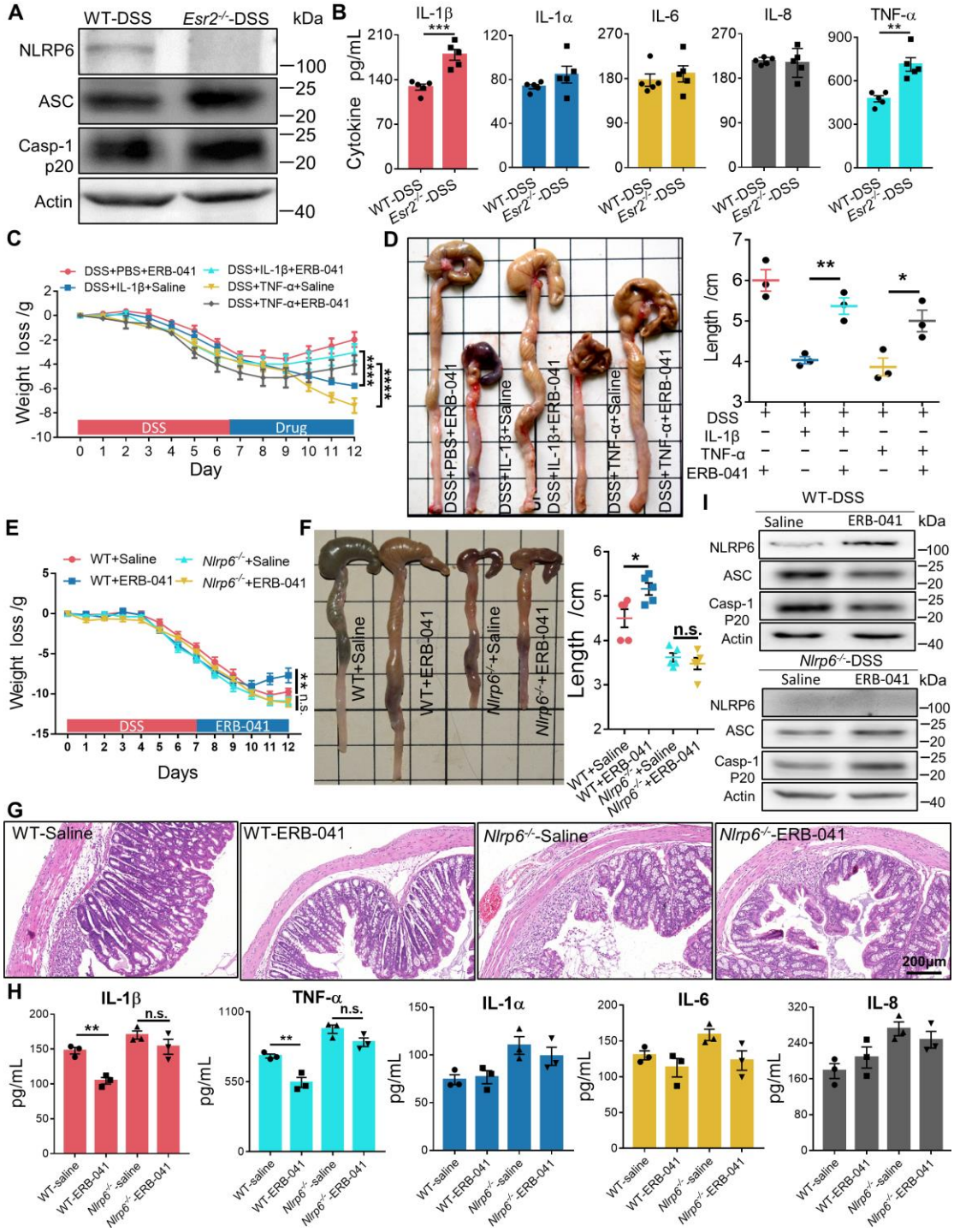

Fig. 1 ERβ inhibits DSS-induced colitis via NLRP6. WT and *Esr2*$^{-/-}$ mice were administered 3% DSS in drinking water for 7 days (n = 5). (A) NLRP6 inflammasome (NLRP6, ASC, and Casp-1 p20) expression of mouse colon homogenate. (B) Tissue IL-1β, IL-1α, IL-6, IL-8, and TNF-α levels were measured by ELISA. The statistics are

910 shown as mean ± SEM. **P<0.01, ***P<0.001, n.s., not significant, by unpaired
911 Student's t-test. WT mice were administered 3% DSS in drinking water for 7 days
912 following intraperitoneal (i.p.) IL-1β (1 μg/kg body weight) or TNF-α (500 ng/kg body
913 weight) with(out) ERB-041 (5 mg/kg body weight) injection for 5 days (n = 3). (C)
914 Weight loss of different mice. Data represent mean values ± SEM. ****P< 0.0001, by
915 two-way ANOVA with Tukey's post hoc test. (D) Gross pathology and length change
916 of colons. The statistics are shown as mean ± SEM. *P< 0.05, **P< 0.01, by unpaired
917 Student's t-test. WT and *Nlrp6*$^{-/-}$ mice were administered 3% DSS in drinking water for
918 7 days followed by intraperitoneal (i.p.) injection of saline or the selective ERβ agonist
919 ERB-041 (5 mg/kg body weight) for 5 days (n = 5). (E) Weight loss of treated mice.
920 Data represent mean values ± SEM. **P< 0.01, n.s., not significant, by two-way
921 ANOVA with Tukey's post hoc test. (F) Representative gross photographs and the
922 colon length of different mice. (G) Representative H&E staining of distal colon sections
923 from mice. (Scale bars, 200 μm). (H) Tissue IL-1β, TNF-α, IL-1α, IL-6, and IL-8 levels
924 were measured by ELISA. The statistics are shown as mean ± SEM. *P< 0.05, **P<
925 0.01, n.s., not significant, by unpaired Student's t-test. (I) NLRP6 inflammasome
926 (NLRP6, ASC, and Casp-1 p20) expression of mice colon homogenate.

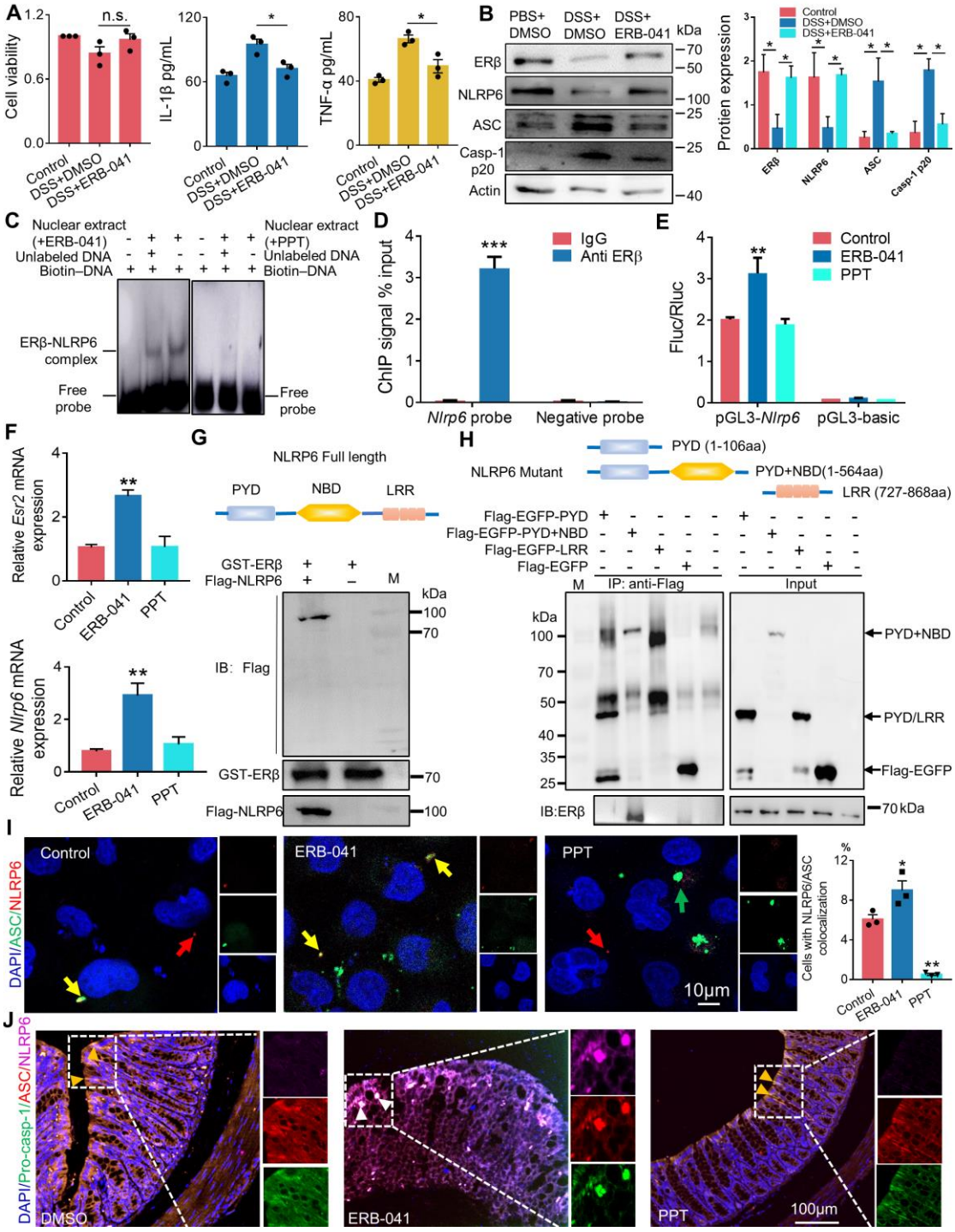

Fig. 2 ERβ activates NLRP6 gene expression and inflammasome assembly in colon epithelial cells and intestinal tissues. Human colon mucosal epithelial cells (NCM-460) were stimulated with 3% DSS for 24 h, then treated by ERB-041 (1 μM) for 48 h. (A) Cell viability of treated cells was detected by the CCK-8 method. Cytokine (IL-1β

and TNF-α) levels in the supernatant determined by ELISA. Each data point represents a unique experiment performed in triplicate. Data represent mean values ± SEM. *P< 0.05, n.s., not significant, by unpaired Student's t test. (B) Immunoblotting of treated cell lysates. Data are representative of three independent experiments. *P< 0.05, by two-way ANOVA with Tukey's post hoc analysis. Normal NCM-460 cells were stimulated with the selective ERβ agonist (ERB-041, 1 μM) and ERα agonist (PPT, 1 μM) for 48 h. (C) Gel-shift assays with the NLRP6 probe and nuclear lysate. (D) Chip-qPCR analysis to determine the relative enrichment of ERβ at the NLRP6 gene promoter region. (E) Luciferase reporter assay to determine the activation the NLRP6 promoter by ER agonists. Each data point represents a unique experiment performed in triplicate. Data represent mean values ± SEM. ***P< 0.001, compared to IgG by two-way ANOVA with Sidak's post hoc analysis. *P< 0.05, **P< 0.01, ****P< 0.0001, compared to control by two-way ANOVA with Tukey's post hoc analysis. (F) qRT-PCR assay for Esr2 and Nlrp6 genes in the NCM-460 cells with ERB-041 or PPT stimulation. Data represent mean values ± SEM. **P< 0.01, by one-way ANOVA with Dunnett's post hoc analysis (vs. Control). (G) In vitro interaction of purified GST-ERβ with Flag-tagged NLRP6 in untreated NCM-460 cells. (H) Co-immunoprecipitation of ERβ with Flag-EGFP-tagged NLRP6 mutant in untreated NCM-460 cells. PYD, pyrin domain; NBD, nucleotide binding domain; LRR, eucine-rich repeat domain. (I) Representative immunofluorescence staining for NLRP6 (red), ASC (green), and DAPI nuclear stain (blue) of NCM-460 cells, treated as ERB-041 or PPT. The yellow arrow represents the co-localization of NLRP6 and ASC. (Scale bars,

954 10 μm). At least 400 cells were analyzed per group. Each data point represents a unique
955 experiment performed in triplicate. Data represent mean values ± SEM. *P< 0.05, **P<
956 0.01, by one-way ANOVA with Dunnett' s post hoc analysis (vs. Control). (J)
957 Representative immunofluorescence staining for NLRP6 (violet), ASC (red), Pro-casp-
958 1 (green), and DAPI nuclear stain (blue) in ERB-041 (5 mg/kg body weight) or PPT (5
959 mg/kg body weight) treated colon tissue. The yellow arrow represents the co-
960 localization of Pro-casp-1 and ASC. The white arrow represents the co-localization of
961 NLRP6, Pro-casp-1 and ASC. (Scale bars, 100 μm).

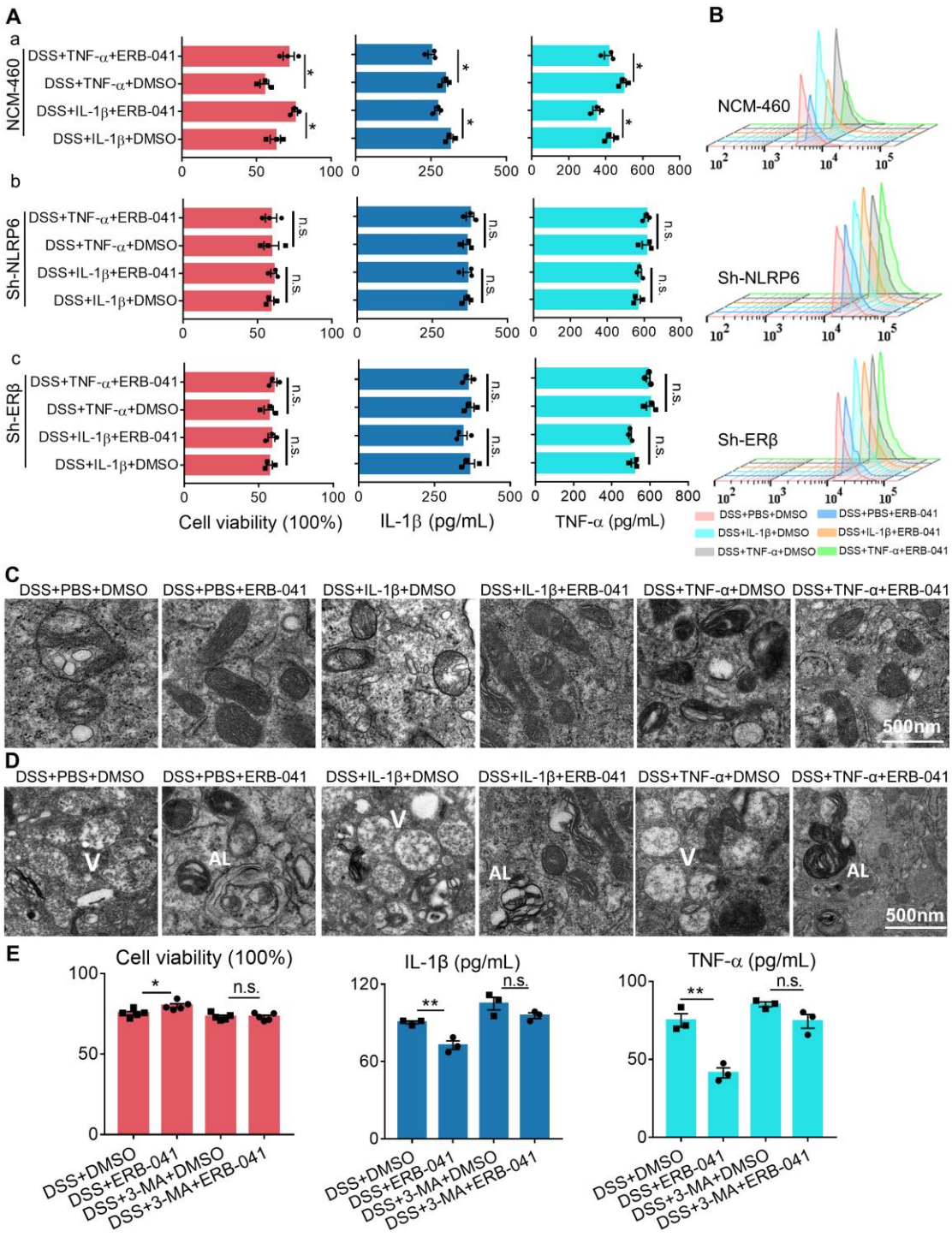

Fig. 3 The role of ERβ and NLRP6 in inflammation, mitochondrial damage, and autophagy. NCM-460 cells (a), NLRP6 knockdown (Sh-NLRP6, b), and ERβ knockdown (Sh-ERβ, c) NCM-460 cells were stimulated with 3% DSS for 24 h, then treated with IL-1β (10 ng/mL) or TNF-α (5 ng/mL) together with or without ERB-041 (1 μM) for 48 h. (A) Cell viability of treated cells was detected by the CCK-8 method.

Cytokines (IL-1β and TNF-α) levels in the supernatant were determined by ELISA. (B) After treatment, cells were incubated with Mito-SOX and then examined by Flow Cytometer. Histograms quantification of ROS positive cells is indicated in Fig. S3B. (C) Representative transmission electron microscope images of mitochondria in different group. (Scale bars, 500 nm). (D) Representative transmission electron microscope images of autolysosome in different groups. (Scale bars, 500 nm). AL: autolysosome, V: vacuole. (E) NCM-460 cells were stimulated with 3% DSS for 24 h, then treated with 3-MA (100 μM) together with or without ERB-041 (1 μM) for 48 h. Cell viability of treated cells was detected by CCK-8 method. Cytokines (IL-1β and TNF-α) levels in the supernatant were determined by ELISA. Each data point represents a unique experiment performed in triplicate. Data represent mean values ± SEM. *P< 0.05, **P< 0.01, n.s., not significant, by unpaired Student's *t*-test.

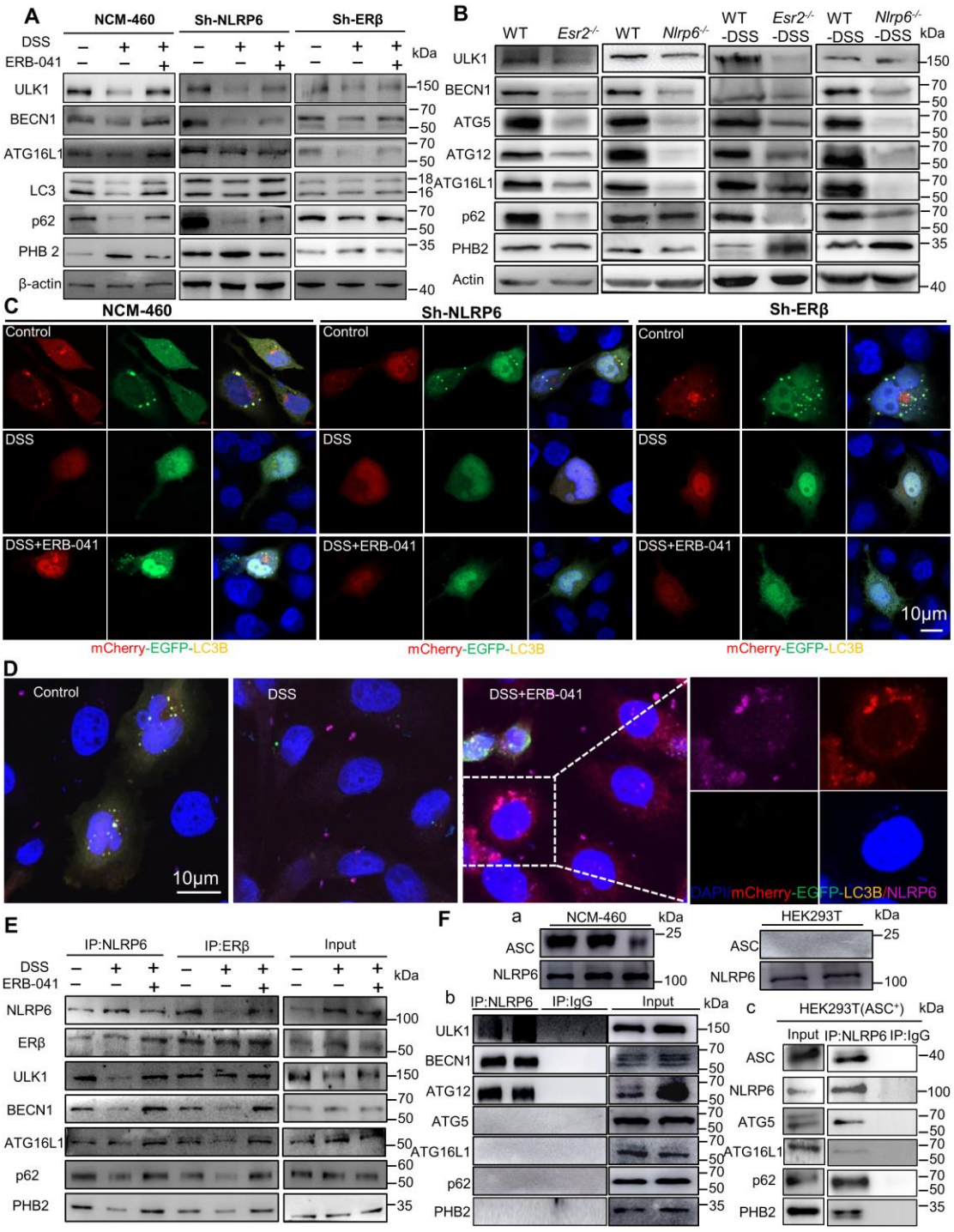

Fig. 4 ERβ-NLRP6 promotes autophagic flux and interacts with autophagy-related proteins. NCM-460 cells, NLRP6 knockdown (Sh-NLRP6), and ERβ knockdown (Sh-ERβ) NCM-460 cells were treated with 3% DSS for 24 h, then treated with ERB-041 (1 μM) for 48 h. (A) Western blots were probed with specific anti-ULK1, anti-BECN1, anti-ATG16L1, anti-LC3, anti-p62, and anti-PHB2 antibodies. (B)

Western blot analysis of colon tissue from WT, *Esr2*$^{-/-}$ and *Nlrp6*$^{-/-}$ mice treated with or without 3% DSS. Western blots were probed with specific anti-ULK1, anti-BECN1, anti-ATG5, anti-ATG12, anti-ATG16L1, anti-p62, and anti-PHB2 antibodies. (C) Confocal microscopy of EGFP-mCherry-LC3B (yellow) expressed in treated NCM-460 cells, Sh-NLRP6, and Sh-ERβ cells. (Scale bars, 10 μm). (D) Confocal microscopy of EGFP-mCherry-LC3B expressed in treated NCM-460 cells, and then immunostained for endogenous NLRP6 (Violet). (Scale bars, 10 μm). (E) Co-immunoprecipitation of autophagy protein with NLRP6 and ERβ in 3% DSS and 3% DSS+ ERB-041 (1 μM) treated NCM-460 cells. (F-a) ASC and NLRP6 expression levels in NCM-460 and HEK293T cells. (F-b) Co-immunoprecipitation of autophagy protein with NLRP6 in HEK293T (ASC^{-}) cells. (F-c) Co-immunoprecipitation of autophagy protein with NLRP6 in HEK293T cells transfected with Flag-EGFP-ASC plasmid (ASC^{+}).

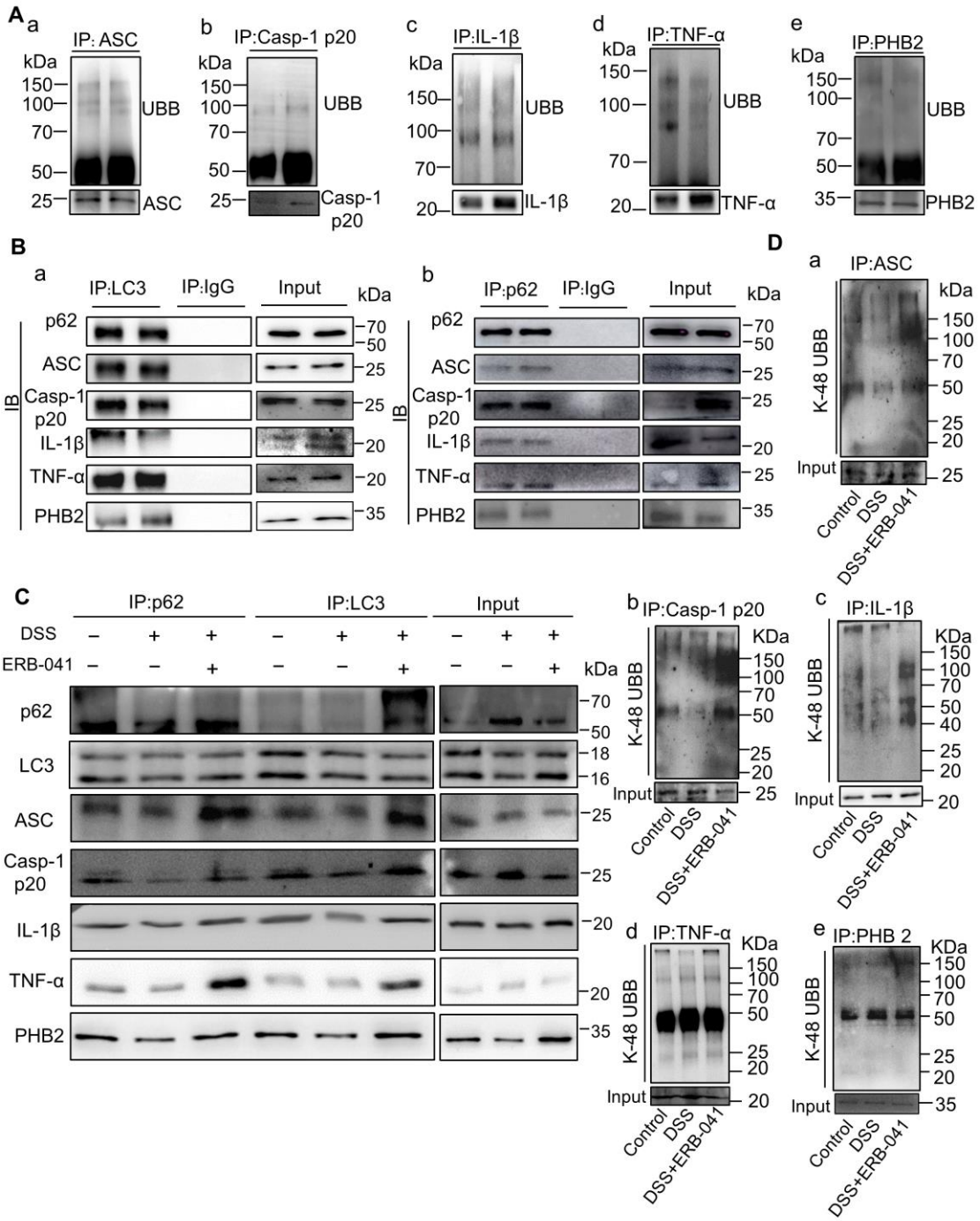

998

999 **Fig. 5 ERβ promotes the eliminattion of the inflammasome, cytokines, and**

1000 **damaged mitochondria.** (A) Polyubiquitination detection of ASC (a), Casp-1 p20 (b),

1001 IL-1β (c), TNF-α (d), and PHB2 (e) in untreated NCM-460 cells. (B) Co-

1002 immunoprecipitation of ASC, Casp-1 p20, IL-1β, TNF-α, and PHB2 with LC3 (a) and

1003 p62 (b) in untreated NCM-460 cells. (C) Co-immunoprecipitation of ASC, Casp-1 p20,

IL-1β, TNF-α, and PHB2 with LC3 and p62 in 3% DSS and 3% DSS+ERB-041 treated NCM-460 cells. (D) K48-linked polyubiquitination detection of ASC (a), Casp-1 p20 (b), IL-1β (c), TNF-α (d), and PHB2 (e) in 3% DSS and 3% DSS+ ERB-041 treated NCM-460 cells.

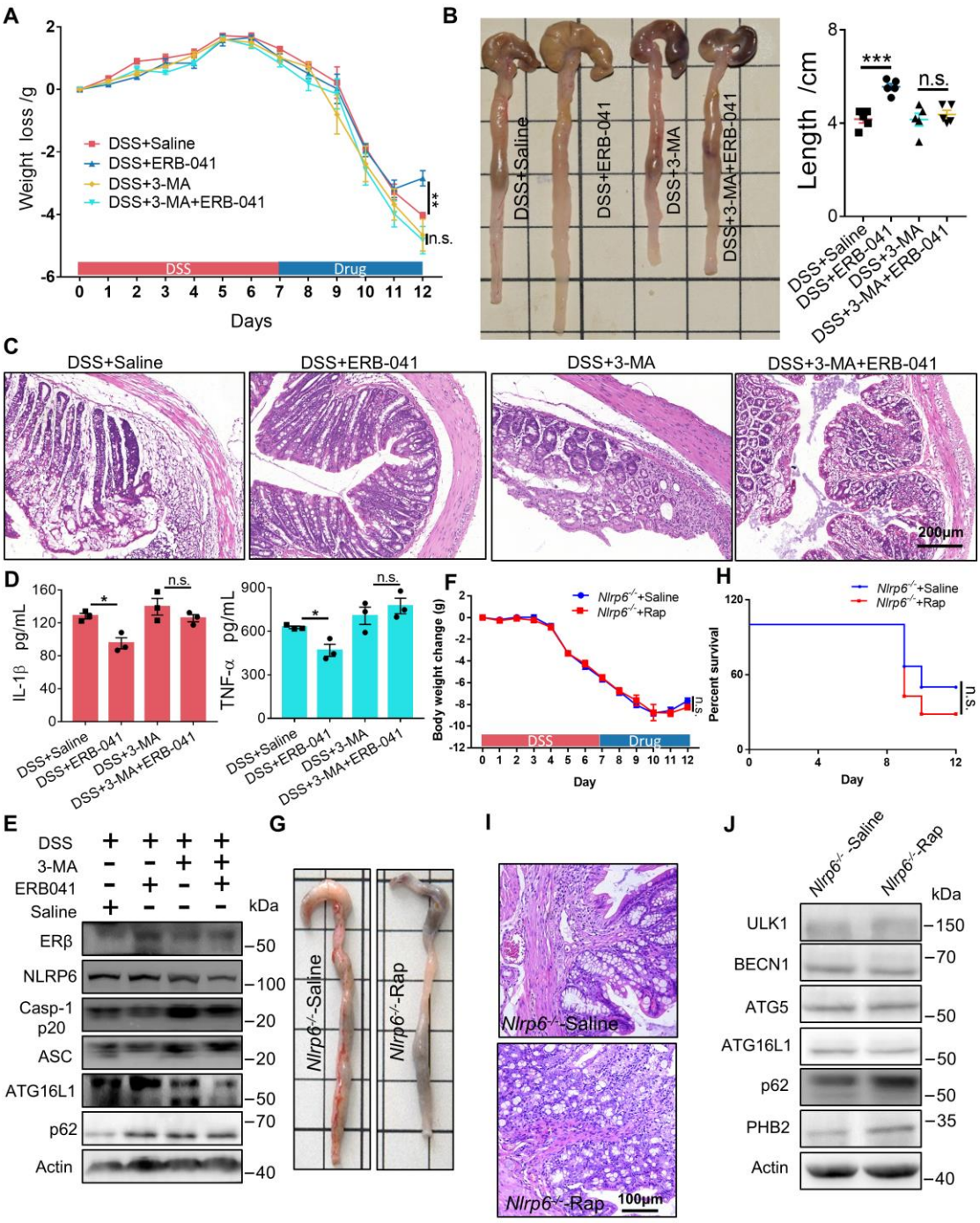

1009

1010 **Fig. 6 NLRP6 is required for Rap-induced recovery from inflammation.** WT mice

1011 were administered 3% DSS in drinking water for 7 days followed by intraperitoneal

1012 (i.p.) injection of saline or the ERB-041 (5 mg/kg body weight) with or without 3-MA

1013 (1.5 mg/kg body weight) for 5 days (n = 5). (A) Weight loss of colitis model mice. Data

1014 represent mean values ± SEM. $^{**}P < 0.01$, n.s., not significant, by two-way ANOVA

with Tukey's post hoc test. (B) Representative gross photographs and the colon length of different mice. (C) Representative H&E staining of distal colon sections from mice. (Scale bars, 200 μm). (D) Tissue IL-1β and TNF-α levels were measured by ELISA. (E) ERβ, NLRP6 inflammasome (NLRP6, ASC, and Casp-1 p20), and autophagy protein (ATG16L1 and p62) expression of mice colon homogenate. The statistics are shown as mean ± SEM. *P< 0.05, ***P< 0.001, n.s., not significant, by unpaired Student's t-test. *Nlrp6*$^{-/-}$ mice were administered 3% DSS in drinking water for 7 days followed by intraperitoneal (i.p.) injection of saline (n = 6) or rapamycin (Rap) (2 mg/kg body weight, n = 7) for 5 days. (F) Weight loss of treated mice. (G) Representative gross photographs and the colon length of different mice. (H) Survival rate of Rap treated-mice compared with that of Saline treated-mice. Data represent mean values ± SEM. n.s., not significant, by two-way ANOVA with Sidak's post hoc test. (I) Representative H&E staining of distal colon sections from mice. (Scale bars, 100 μm). (J) Autophagy protein expressions of mice colon homogenate.

Supplementary Files

This is a list of supplementary files associated with this preprint. Click to download.

- MovieS1.avi
- MovieS2.avi
- MovieS3.avi
- MovieS4.avi
- MovieS5.avi
- MovieS6.avi
- MovieS7.avi
- MovieS8.avi
- MovieS9.avi
- MovieS10.avi
- MovieS11.avi
- MovieS12.avi
- MovieS13.avi
- MovieS14.avi
- MovieS15.avi
- MovieS16.avi
- MovieS17.avi
- MovieS18.avi
- TableS1.xlsx
- TableS2.xlsx
- SupplementalMaterial.pdf